Helsinki University of Technology Publications in Engineering Physics
Teknillisen korkeakoulun teknillisen fysiikan julkaisuja
Espoo 2004 TKK-F-A827

MASS TRANSPORT IN POLYMER ELECTROLYTE MEMBRANE FUEL CELLS USING NATURAL CONVECTION FOR AIR SUPPLY

Tuomas Mennola

Dissertation for the degree of Doctor of Science in Technology to be presented with due permission of the Department of Engineering Physics and Mathematics for public examination and debate in Auditorium F1 at Helsinki University of Technology (Espoo, Finland) on the 2nd of April, 2004, at 12 o'clock noon.

Helsinki University of Technology
Department of Engineering Physics and Mathematics
Laboratory of Advanced Energy Systems

Distribution:
Helsinki University of Technology
Laboratory of Advanced Energy Systems
P.O. Box 2200
FIN-02015 HUT
Tel. +358-9-451 3198
Fax. +358-9-451 3195
E-mail: Tuomas.Mennola@hut.fi

ISBN 951-22-6983-X
ISBN 951-22-6984-8 (pdf)

ISSN 1456-3320
ISSN 1459-7268 (pdf)

Otamedia Oy
Espoo 2004

HELSINKI UNIVERSITY OF TECHNOLOGY
P.O. BOX 1000, FIN-02015 HUT
http://www.hut.fi

ABSTRACT OF DOCTORAL DISSERTATION

Author Tuomas Mennola

Name of the dissertation
MASS TRANSPORT IN POLYMER ELECTROLYTE MEMBRANE FUEL CELLS USING NATURAL CONVECTION FOR AIR SUPPLY

Date of manuscript 20.10. 2003 | Date of the dissertation 2.4. 2004

☐ Monograph ☑ Article dissertation (summary + original articles)

Department Engineering Physics and Mathematics
Laboratory Advanced Energy Systems
Field of research Fuel cells
Opponent(s) Prof. Göran Lindbergh
Supervisor Prof. Peter Lund
(Instructor)

Abstract

A fuel cell converts chemical energy into electricity and heat through electrochemical reactions. Polymer electrolyte membrane fuel cells (PEMFCs) are approaching commercialization in many applications, including transportation, stationary power, and portable devices. In this thesis, the focus was on small-scale PEMFCs, in which natural convection is used as the air supply method.

A cell design with straight vertical cathode channels was studied using experimental and modeling methods, in order to obtain a quantitative insight into mass transport phenomena and to identify the performance limiting processes. The variation of mass transport conditions over the active area of the cell was studied using a current distribution measurement system, which was based on the use of a segmented current collector. The accuracy of the method was analyzed by experimental work and numerical simulation. In order to quantify the local mole fractions of water and oxygen, and the velocity of buoyancy-driven air flow in the cathode channel, a numerical model was developed to describe mass transport in the cathode channel and the gas diffusion layer. Water transport across the polymer membrane was studied by measuring the fraction of product water exiting through the anode. The results give indication of the variation of net water transport coefficient across the active area. The redistribution of water along with the hydrogen flow was also observed. The effect of ambient temperature and relative humidity on cell performance was investigated in a climate chamber. For stack research, a measurement approach was developed for determining the ohmic voltage losses of individual cells in a stack by the current interruption method.

As an overall conclusion, it was found that the cell design should be improved especially from the point of view of water management. In order to reduce flooding problems, the cross-section and length of the cathode channels were identified as key parameters to be optimized. It was also found that mechanically rigid gas diffusion layer materials are advantageous for designing an optimized geometry. In addition, it was found that the choice of the anode flow geometry can be used to control the distribution of water across the active area.

Keywords PEMFC, cathode, natural convection, water management, current distribution, modeling, current interruption

UDC 66.021.3:541.13 | Number of pages 63 + app. 49

ISBN (printed) 951-22-6983-X | ISBN (pdf) 951-22-6984-8

ISBN (others) | ISSN 1456-3320 (printed), 1459-7268 (pdf)

Publisher Department of Engineering Physics and Mathematics

Print distribution Laboratory of Advanced Energy Systems, P.O. Box 2200, 02015 HUT, Finland

☑ The dissertation can be read at http://lib.hut.fi/Diss/ 2004/isbn9512269848/

Preface

The work described in this thesis was carried out in the Laboratory of Advanced Energy Systems in Helsinki University of Technology, during the years 1998-2003. This has been a period of great progress and growth in fuel cell research, and it has been exciting to be a part of it. The work was done under the supervision of Prof. Peter Lund, whom I thank for providing an opportunity to work on this fascinating subject. The completion of this thesis has been made possible and meaningful by a large number of people, most notably the other members of the fuel cell research group of our laboratory. I am greatly indebted to Matti Noponen, Mikko Mikkola, Tero Hottinen, Mikko Aronniemi, and Olli Himanen for their contributions to this work. Outside our group, Tanja Kallio from the Laboratory of Physical Chemistry and Electrochemistry has been an invaluable source of support throughout the years. I owe my gratitude to all of you for collaboration and co-authorship. I also want to express my deep appreciation to Janne Kaskimies, whose work during the first two years of our fuel cell research was essential in laying the foundation for the later achievements of me and others. The rest of the staff of our laboratory have created a pleasant and inspiring atmosphere to work in, and provided many forms of support, both scientific and otherwise, throughout these years.

Outside our laboratory, my network of collaboration has expanded to include numerous individuals and organizations both in Finland and abroad. This has allowed me to greatly expand my world-view and get to know some truly extraordinary people. It is not possible to mention everyone here by name, so I wish to extend thanks to all of you collectively. I hope that you recognize yourselves and know that your support is highly valued.

The National Technology Agency of Finland is gratefully acknowledged for providing continuous funding for our research. In addition, I wish to thank SGL CARBON GmbH and Labgas Instrument Company for supplying materials, which have been used in the experimental work of this thesis, and CSC - Scientific Computing Ltd. for providing computational resources for the simulation work.

Finally, I want to thank my parents and my sister for their support and understanding.

Tuomas Mennola

List of publications

This thesis is an introduction to the following publications:

I M. Noponen, T. Mennola, M. Mikkola, T. Hottinen, and P. Lund, ”Measurement of current distribution in a free-breathing PEMFC”, *J. Power Sources* **106** (2002) 304-312.

II T. Mennola, M. Noponen, M. Aronniemi, T. Hottinen, M. Mikkola, O. Himanen, and P. Lund, ”Mass transport in the cathode of a free-breathing polymer electrolyte membrane fuel cell”, *J. Appl. Electrochem.* **33** (2003) 979-987.

III T. Mennola, M. Noponen, T. Kallio, M. Mikkola, and T. Hottinen, ”Water balance in a free-breathing polymer electrolyte membrane fuel cell”, *J. Appl. Electrochem.* **34** (2004) 31-36.

IV T. Hottinen, M. Noponen, T. Mennola, O. Himanen, M. Mikkola, and P. Lund, ”Effect of ambient conditions on performance and current distribution of a polymer electrolyte membrane fuel cell”, *J. Appl. Electrochem.* **33** (2003) 265-271.

V T. Mennola, M. Mikkola, M. Noponen, T. Hottinen, and P. Lund, ”Measurement of ohmic losses in individual cells of a PEMFC stack”, *J. Power Sources* **112** (2002) 261-272.

VI T. Hottinen, M. Mikkola, T. Mennola, and P. Lund, ”Titanium sinter as gas diffusion backing in PEMFC”, *J. Power Sources* **118** (2003) 183-188.

In Publication I, a measurement system for current distribution measurements is introduced. The system was designed and constructed in order to gain understanding of mass transport phenomena and performance limiting factors, and to facilitate the optimization of the use of the active area in the cell. These issues are developed further in Publications II-IV. In Publication II, a modeling approach is presented, with the particular aim of predicting the mole fractions of oxygen and water vapor, and the flow velocity in a cathode channel of a natural convection cell. As an outcome of the modeling study, the need arose to quantify the transport of water through the polymer electrolyte membrane of the cell. This was investigated experimentally in the study reported in Publication III. In Publication IV, the effect of ambient conditions on the performance of the cell was investigated by placing the current distribution measurement system in a climate chamber. In Publication V, a method is introduced for the measurement of the ohmic losses of individual cells in a stack. This was accomplished using the current interruption method. In Publication VI, a preliminary study is reported on the use of titanium sinters as a mechanically rigid gas diffusion material.

The scientific work reported in this thesis is the outcome of co-operation. The author has taken the main responsibility of the work reported in Publications II, III, and V, including the design of experimental facilities, designing and performing the measurements, analyzing the results, and writing the publications. In Publication I, the author has participated actively in the design of the experiments and the analysis of the results. He has also performed the simulation work included in the publication, and written parts of the publication. In the work reported in Publications IV and VI, the author has participated in the design of the experiments and discussing the results, and

participated in the writing of the publications by offering comments and suggestions. In addition, the author has participated in the construction of the experimental facilities used in the work of Publication IV.

Contents

1 Introduction

1.1 Background

The fuel cell is an electrochemical device that converts the chemical energy of its reactants directly into electricity and heat, without combustion. Fuel cells have a substantial range of potential applications, on a power scale from less than a watt to megawatts. In transportation, fuel cells hold the potential to end the century-long reign of internal combustion engines. In stationary energy production, fuel cell power plants may have a key role in the transition of the energy economy toward a more distributed, network-type structure. Fuel cells could also replace batteries in many small-scale applications. Important technical breakthroughs in fuel cell technology have been achieved especially during the past decade, and as a result, several of these applications, which not a long ago appeared quite far removed from reality, are now rapidly approaching commercialization.

The development of fuel cell technology has been accelerated by the increasingly acute need for cleaner and more efficient energy conversion methods. Environmental problems due to energy production and transportation are growing. This is the result of the combination of population growth and economic growth, particularly in the third world. Furthermore, it appears unlikely that the increase in global energy consumption could be brought to a halt any time soon. The danger that the release of carbon dioxide into the atmosphere may adversely affect the climate of our planet is becoming recognized as real. Therefore, there is an urgent need for cleaner energy technologies. Conventional energy conversion methods, however, are approaching their efficiency limits. Therefore, fuel cell technology is receiving growing interest and research efforts.

Fuel cells also have the important benefit that their efficiencies are not significantly affected by the size of the cell. In this respect, fuel cells are different from energy conversion methods that rely on heat engines, such as turbines and internal combustion engines, in which efficiencies generally decrease with decreasing size. Fuel cells are regarded as a promising new power source for many small applications, which are currently powered by batteries. Major breakthroughs in battery technology are not in sight, and therefore, there is a growing need to develop new power sources to meet the increasing power demand of electronic devices. Small applications are also seen as an important initial step toward the market entry of fuel cells, even though their direct impact on the energy economy is not large.

The fuel cell type studied in the present thesis is the polymer electrolyte membrane fuel cell (PEMFC). The advantages specific to the PEMFC are high power density, quick start-up, rapid response to load changes, and the potential for reaching low production costs. Because of its all-solid construction, the stability and leakage problems typical of liquid electrolytes are avoided. In this thesis, experimental and theoretical studies on PEMFCs were carried out, with emphasis on small applications, which have, until very recently, received only a minor part of worldwide research efforts devoted to the development of fuel cells. A major aim of the work was to achieve a better understanding of mass transport phenomena in a fuel cell that operates using natural convection as the air supply method.

1.2 Motivation and objectives

Fuel cells have many potential small-scale applications, such as portable computers, mobile phones, power tools, and telecommunication base stations. The power consumption of portable electronic devices is growing because of new features and increased computing power. Currently, these devices are powered by various types of primary and rechargeable batteries. The limitations of battery capacity are one of the most significant sources of dissatisfaction for the users of laptop computers [1]. In addition, discarded batteries often become harmful waste due to the toxic substances present in them.

Both batteries and fuel cells produce electricity through electrochemical reactions. However, the fundamental difference is that a fuel cell is only an energy conversion device, whereas a battery is a conversion and storage device at the same time. Energy is stored in a battery in the form of substances that are consumed in the electrochemical reactions. The depletion of the reacting substances or the accumulation of reaction products will eventually cause the energy delivery from the battery to cease. The battery must then be either recharged or replaced. In a fuel cell energy system, the conversion and storage functions are decoupled, and therefore, the power and energy capacities can be separately optimized. In addition, a fuel cell system can be rapidly refueled, as opposed to the slow recharging of batteries.

The technology of small fuel cells is significantly less established than that of larger fuel cells. The challenges of designing useful fuel cell power sources for small applications include the miniaturization of the system, achieving high power and energy density, and ensuring reliable and efficient operation. Simplicity of the system is desirable, and therefore, natural convection is an attractive air supply method. Natural convection is gravitationally induced fluid movement, which is caused by density differences within the fluid. On the cathode side of a PEMFC, density differences arise as a result of temperature gradients and composition changes. Because natural convection does not depend on the use of auxiliary devices, it is an attractive option for simplifying the fuel cell system. Even if an auxiliary fan is used to feed air at peak power, natural convection enables startup without auxiliary power, and it increases the reliability of the system, because a failure of the fan does not lead to complete loss of power. However, operating the cell on natural convection also means that effective and reliable air supply must be ensured using passive means, *i.e.* methods that rely on the choice of the geometry and materials of the cell.

The specific questions treated in this thesis were defined as a result of problems that had arisen as a result of initial experiments on free-breathing cells[1] in the Laboratory of Advanced Energy Systems. It had become apparent that the present understanding on mass transport in a free-breathing cell was insufficient to reliably identify the performance limiting causes and to propose improvements of the cell design. The transport of oxygen and water can be expected to profoundly influence the operation of the cell. However, due to the spontaneous nature of natural convection, the small magnitudes of the mass flows, and the relatively small dimensions of the cell structure, these phenomena are difficult to observe and to quantify. The goal of the present thesis was set to achieving a comprehensive picture of mass transport and its effects on cell performance in a fuel cell operating on natural convection. In order to accomplish this,

[1] The terms “free-breathing cell” and “natural convection cell” are used interchangeably in this thesis.

a variety of new applications of measurement techniques and modeling methods were developed to elucidate mass transport inside a fuel cell. The work concentrated mainly on the cathode (air) side of the cell, because the cathode is normally the largest source of losses in a hydrogen-powered fuel cell.

1.3 Outline of this thesis

The thesis begins with an introduction to fuel cells in Chapter 2. The specific topics covered include the operating principles, main functional parts, polarization behavior, and efficiency of a PEMFC. Mass transport phenomena, water balance, and heat management in the cell are also discussed. Special emphasis is placed on issues specific to small fuel cells. The history and trends in fuel cell technology development are briefly covered, and an overview of other types of fuel cells is given.

Both experimental and modeling methods were utilized during the work. An overview of the methods is given in Chapter 3. The fuel cell test station that served as a foundation of the measurement setups is described, and the principles and implementation of the special measurement techniques are discussed. The main measurement techniques were the current interruption method, which provides information on ohmic losses, the segmented current collector that was used to measure current distributions, and a water collection setup to measure water transport. Climate chamber measurements, from which additional data was obtained, are briefly covered. In addition to the experimental work, a mass transport model of the cathode side of a free-breathing fuel cell was developed. The main features and assumptions of the model are discussed.

The results obtained using each of the measurement techniques, as well as modeling work, are described in Chapter 4. The most important results are presented and discussed, the interconnections among the subject areas are highlighted, and the consequences and restrictions of the results are evaluated. The verification of the reliability of the current distribution measurement system is discussed first, followed by the sub-tasks in which the measurement system was utilized. These were the water transport measurements, the climate chamber measurements, and the modeling study, in which experimentally obtained current distributions were used to determine boundary conditions for the model. In addition to these, the use of the current interruption method for the investigation of individual cells in a fuel cell stack is presented, and results from the characterization of titanium sinter materials for gas diffusion layers are reviewed. A summary of the main results of the thesis is given in Chapter 5.

2 Fuel cells

2.1 History and major trends of fuel cell technology

The fuel cell is an old innovation, which has taken a long time to mature to the threshold of widespread commercialization. The innovation is usually credited to Sir William Grove, who in 1839 reported an electrochemical cell of a novel type. The innovation arose from his experiments with electrolysis, which can be considered the reverse process for fuel cells. A more extensive review on the early history of fuel cells can be found in [2].

This work deals with a class of fuel cells that uses proton conductive polymers as the electrolyte. The first PEMFCs were developed by General Electric Company in the 1950's. They were used as power sources in the Gemini spacecraft. Initially, the applications of PEMFCs were limited to space systems and other special applications, where fuel cells have significant technical advantages over alternative solutions and high cost can be tolerated. The Nafion® membrane, which was developed in the 1960's by E.I. DuPont de Nemours & Company, brought a substantial increase to the lifetime of the cell, which was a problem in early PEMFCs.

However, it was not until the late 1980's when this fuel cell type became a viable candidate for more earthly applications. This was made possible by fundamental technical breakthroughs, most notably the reduction of the platinum contents needed in the electrodes, that enabled costs to be decreased to levels that made the serious development of the PEMFC worthwhile. Two of the most important drivers of technology development during the recent years have been the needs of the transportation and distributed energy sectors.

Fuel cells as power sources of electrical vehicles have been subject to extensive research efforts. Transportation holds a large and growing share of world energy consumption, and it is currently powered almost exclusively by oil products. Battery-powered electric vehicles are unlikely to reach the performance and operating range of vehicles that are powered by internal combustion engines. Hydrogen and fuel cells thus appear as the best way of creating a sustainable transportation system. The high efficiency of fuel cells on partial load makes them particularly favorable as vehicle power sources, because most vehicles operate on a fraction of the peak power of the engine for the majority of time. Small fleets of fuel cell electric vehicles are currently under field testing, and the prospects for their wider market introduction during this decade appear favorable. This is especially true in the case of hydrogen-fueled fuel cell buses, for which market introduction is not dependent on the development of a widespread service station network.

Fuel cells are also seen as promising in stationary power production. Fuel cells may enable efficient and economical power generation in smaller units than what has been possible using conventional technology. The present-day energy infrastructure is mostly based on large central power stations and hierarchical distribution networks, but there is a long-term trend toward distributed and small-scale power generation. In industrial countries, the growth of energy consumption is relatively slow, and the introduction of free energy trade has made it difficult to predict the development of

energy markets far into the future. For these reasons, power production that can be constructed rapidly and in small units becomes preferable over large central power stations. In the developing countries, on the other hand, small power stations, which are located near the consumption, are beneficial, because the national electricity distribution grid may be relatively undeveloped. On the long term, hydrogen and fuel cells can also be seen as a key to the large-scale integration of renewable energy sources into the energy economy.

In addition to the above mentioned sectors, small-scale portable and stationary applications are emerging as a possibly very large market for fuel cell products. Until recently, they have only received a minor share of all research efforts devoted to fuel cells, but they are currently attracting increasing R&D investments. Small fuel cells are not yet mature for consumer markets, but promising progress is being made. The present work aims to contribute to this development.

2.2 The Polymer Electrolyte Membrane Fuel Cell

2.2.1 Overview

In principle, a fuel cell is a remarkably simple device. Electrochemical reactions occur at two reaction sites, which are called the electrodes. On one electrode, an oxidation reaction takes place. This electrode is called the anode. On the other electrode, which is called the cathode, a reduction reaction takes place. As a result of the interphase potentials on the electrodes, a potential difference is formed between them. They are separated by an electrolyte, which conducts ions between the electrodes while separating the reacting species from each other. The electrolyte must also be electronically insulating. The cell can be used as a source of electrical current by connecting the electrodes to an external load. The electrons liberated in the anode reaction are consumed in the cathode reaction. Respectively, the ions liberated in one of the electrode reactions are consumed in the other reaction.

In a PEMFC, the anode reaction is the oxidation of hydrogen, and the cathode reaction is the reduction of oxygen. Water is formed on the cathode as a by-product of the reaction. The half-cell reactions and the total reaction in a PEMFC are given below.

Anode: $H_2 \rightarrow 2H^+ + 2e^-$

Cathode: $\frac{1}{2}O_2 + 2e^- + 2H^+ \rightarrow H_2O$

Total reaction: $\frac{1}{2}O_2 + H_2 \rightarrow H_2O$

The operating principle of a PEMFC is described in Figure 1, and the main functional parts of a unit cell are illustrated in Figure 2. Each of them is given a discussion in the next sub-chapters. The functions of the parts are described, and the required material properties and design considerations discussed.

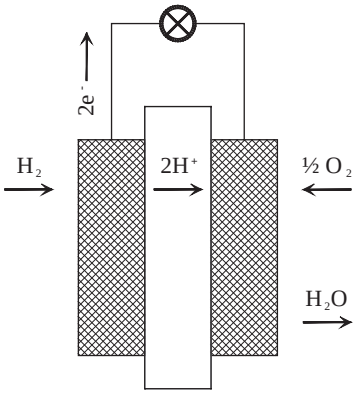

Figure 1. *The operating principle of a PEMFC.*

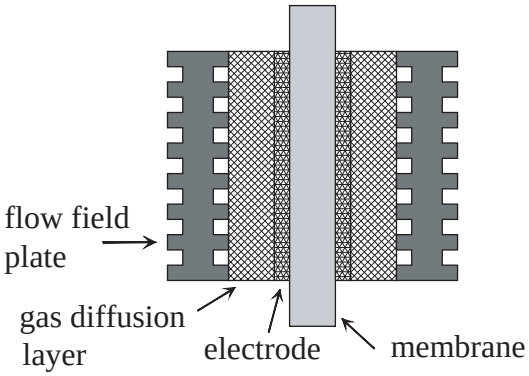

Figure 2. *The main functional parts of a PEMFC. The scale of the picture has been distorted to emphasize the main features.*

2.2.2 Membrane

The membrane can be characterized as an acidic electrolyte, in which the negative ions are immobilized in a polymer matrix. A good membrane material for a PEMFC should have a high protonic conductivity, good chemical and mechanical stability, small water permeability, and low cost. In addition, it should be electronically insulating and not permeable for H_2 and O_2 gases.

The most widely used membrane material is Nafion® by E.I. DuPont de Nemours & Company. The polymer structure consists of a poly(tetrafluoroethylene) backbone, which has side chains ending with sulfonic acid groups. Nafion membranes are available in various thicknesses ranging from 51 to 254 μm. Nafion and other commonly used membrane materials require hydration in order to be proton conductive. The resistance of the membrane is a major contributor to the total ohmic loss of the cell, and the reduction of conductivity due to drying may significantly decrease the performance of the cell. Because of the hydration requirement, the operation temperature range of PEMFCs using common membrane materials is limited in the upper end by the dehydration of the membrane as a result of evaporation.

Extensive research is underway by several research groups to create new membrane materials. Trends in membrane research are reviewed in [3] and [4]. Important goals of

membrane research are lowering costs and discovering materials that would enable operation above the boiling point of water.

In the experimental work reported in this thesis, composite micro-reinforced membranes of W.L. Gore & Associates were used. The composite structure of these membranes provides durability while allowing very thin membranes to be produced [5]. Thin membranes are well suited for small applications, because they can be maintained in a hydrated state using product water of the cell reaction only. The thicknesses of the membrane grades used in the work of this thesis were 25 and 35 μm.

2.2.3 Electrode

The electrodes of a PEMFC typically contain noble metal catalyst, in order to achieve a sufficient reaction rate at low temperatures. Platinum offers the best performance when pure hydrogen is used as fuel, but the addition of other noble metals may enhance the tolerance of the catalyst against fuel impurities. Ruthenium is commonly used for this purpose.

For useful current densities to be obtained, the electrode needs to have a high real surface area compared to the geometric area of the electrode. In order to be in effective use, the catalyst particles must be located in such way that they form a three-phase boundary, *i.e.* they are in contact with both electronic and protonic conductors, and there are free passages for the reactant to reach the catalyst site, and for water transport. The proton conducting phase contained in the electrode region must be hydrated in order to be proton conductive, similarly as the bulk membrane phase.

Because of the high cost of the noble metals, it is essential to achieve a low noble metal content in the electrodes. For this reason, thin-film electrodes are regarded as the optimal solution. The thin-film electrode is a porous layer consisting of proton conducting phase and high surface area carbon black particles with smaller platinum particles attached to them [6]. Typical electrode thicknesses are of the order of micrometers, and the platinum contents are in the range of 0.1-0.4 mg cm^{-2}. The electrode is formed on the membrane surface by spraying, decaling, or other suitable manufacturing method. Research on manufacturing methods has been reviewed in [4].

The entity consisting of the membrane and the electrodes is usually called the membrane electrode assembly (MEA). The thickness of the MEA is only some tens to hundreds of micrometers, depending on the type of membrane used. Because of this extremely compact structure, the power density of a PEMFC can be very high. Therefore, the PEMFC is usually regarded as superior compared with other fuel cell types in applications in which power density is a prime consideration, most notably in transportation and portable applications.

The experimental work reported in this thesis was performed using PRIMEA® MEAs from W.L. Gore & Associates. Their electrodes are of the thin-film type, containing 0.3 or 0.4 mg cm^{-2} of platinum per electrode, depending on the MEA grade used.

2.2.4 Gas diffusion layers

In an assembled fuel cell, the MEA is sandwiched between porous gas diffusion layers. The purpose of the gas diffusion layers is to form an electronic and thermal contact between the electrodes and the flow field plates, and to provide transport paths for the reactant gases and water. The desirable properties for a gas diffusion layer material are high electrical and thermal conductivity, high porosity, an optimal combination of hydrophobic and hydrophilic properties, good chemical and mechanical durability, and low cost. Typical gas diffusion layer materials are carbon-based papers, felts, or cloths. For achieving an optimal combination of properties, several authors recommend a structure that consists of a macroporous backing layer and a microporous diffusion layer applied on one or both sides of the backing layer [7-10]. The typical thickness of commercially available materials is in the range of 300-400 μm. In the majority of the experimental work of this thesis, the gas diffusion materials were of the ®SIGRACET series by SGL CARBON GmbH.

Gas diffusion layer materials, related characterization methods, and recent research have been reviewed by Mathias *et al.* [11]. According to them, *ex-situ* methods for material characterization appear relatively well established, but the correlation of material parameters from *ex-situ* measurements to actual fuel cell performance is still poorly understood. The selection of an optimal material still needs to rely primarily on trial and error. The need for further research on gas diffusion layers is particularly acute from the point of view of small applications, in which reliable and efficient operation must be achieved while relying as much as possible on passive solutions, such as the choice of cell materials.

Before the introduction of thin-film electrodes, the catalyst was usually impregnated into the gas diffusion layer, resulting in a structure know as a gas diffusion electrode. This approach has been found to result in ineffective use of noble metals and weaker contact between the electrode and the membrane. Therefore, gas diffusion electrodes have mostly been abandoned in favor of thin-film electrodes, which also are regarded as better suited for mass-manufacturing.

In addition to traditional carbon based gas diffusion layers, sinter or mesh-type metallic materials may be advantageous in some applications. The mechanical rigidity of metallic materials may open up new possibilities in cell design, because the material does not require the same degree of mechanical support as carbon papers and cloths. The rigidity of metallic materials is also advantageous in normal cell designs, because the gas diffusion layers are under compression in an assembled fuel cell. Carbon-based materials are easily deformed, resulting in reduced porosity and weaker mass transport, whereas metallic materials can withstand high compression loads without reduction in porosity.

Metallic materials, however, have their own characteristic problems. Their conductivity, most notably at the material interfaces, is usually weaker than that of high-quality carbon-based materials. Non-noble metals are prone to corrosion problems, whereas the use of noble metals is limited by their cost. For these reasons, carbon-based materials have traditionally been chosen for PEMFCs. However, only few published studies exist on the use of metallic gas diffusion layers in fuel cells [12-14]. It is possible that they hold unutilized potential, which is becoming more relevant due to the growing interest in small fuel cells.

2.2.5 Flow field plates

The MEAs and the gas diffusion layers are normally located between flow field plates, which typically have channels on the surfaces facing the gas diffusion layers. The channels provide a passage for the distribution of the reactant gases to the electrodes and the removal of product water. The flow field plates also act as separators of reactants, form the electrical connection between unit cells, and function as the mechanical supporting structure of the cell.

The channel geometry of the flow field plates significantly affects the effectiveness of mass transport inside the cell. The optimum channel geometry may be different on different sides of the cell. The choice of geometry is more critical on the cathode side, because the reaction water is produced on the cathode and because the diffusivity of oxygen is significantly lower than that of hydrogen. As shown later in the thesis, however, the flow geometry of the anode side may also have important implications on water distribution over the active area of the cell.

In the optimization of the channel geometry, a balance between a number of conflicting requirements must be sought. The channels of the plate should distribute the reactant gases effectively to the active electrode region. On the other hand, the flow field plate should offer mechanical support for the MEA and provide passages for electronic current and heat. For the optimization of the width and depth of the channels, and the width of the ribs between them, the following guidelines can be given:

- Minimizing the width of the ribs between the channels improves mass transport in the gas diffusion layer in the regions adjacent to the ribs. These regions are problematic from the point of view of mass transport, because the transport path from the channel to these regions is longer than to the regions adjacent to the channels. In addition, the porosity of the gas diffusion layer may be reduced in the regions adjacent to the ribs as a result of the contact pressure exerted by the ribs. Decreasing the ratio of rib width to channel width, however, increases the contact pressure against the gas diffusion layer, which may increase the loss of porosity.
- Decreasing the channel cross-section increases the flow velocity and pressure loss at a given mass throughput rate, which helps to remove water droplets. This must be balanced against the power consumption of the air supply system.
- If air is supplied to the cathode by natural convection or with a fan, low resistance to flow is required, and the optimum cross-section is, therefore, larger than when a compressor or a pump is used. The upper limit for the width of the channels is set by the requirement to provide mechanical support for the MEA. The limit is thus dependent on the rigidity of the gas diffusion layer. Increasing the depth of the channels also reduces flow resistance, but at the expense of increasing the thickness of a unit cell.

From the above mentioned guidelines it is evident that a rigid non-compressible gas diffusion layer material provides more freedom in the design of the flow field geometry, compared to traditional, easily deformed, carbon-based materials. This is of particular importance in free-breathing fuel cells, in which wide channels can be expected to be advantageous.

The research reported in the present thesis focused on a cathode channel geometry that consists of parallel straight channels which have their ends open to the ambient air, enabling the use of natural convection to supply air to the cathode. The geometry of the

cell is illustrated in Figure 3. This type of channel geometry is a well known solution for constructing small, free-breathing cells. However, little research has been done on mass transport phenomena in this type of cells and the optimization of the cell structure. In the few existing studies, mainly whole-cell variables have been measured, with no direct information on local conditions inside the cell [15]. Previous theoretical studies have been limited to the prediction of current-voltage characteristics by analytic equations [16].

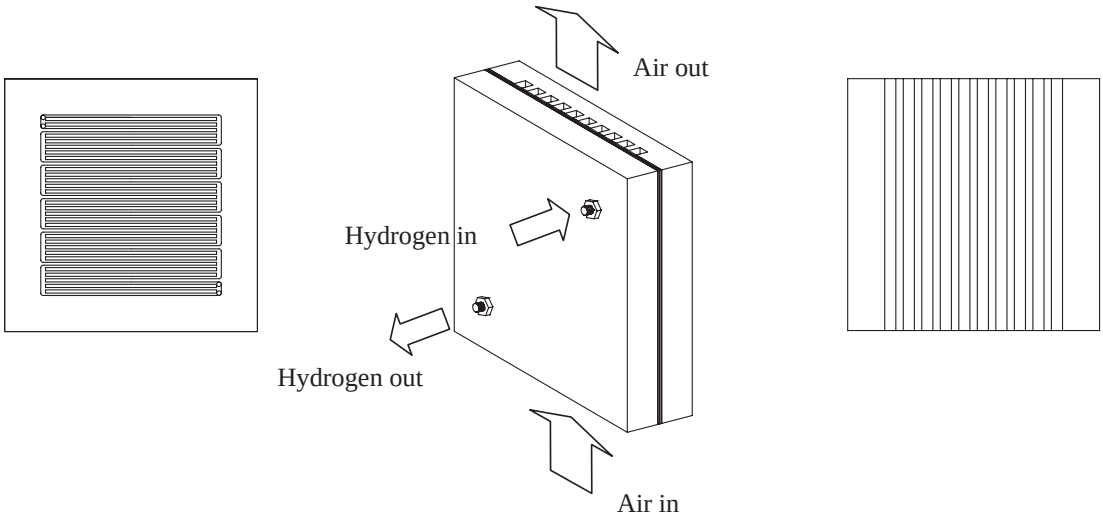

Figure 3. *A free-breathing single cell. Plane views of the anode (left) and cathode (right) flow fields and a spatial view of the assembled cell (middle) are shown.*

The material used for flow field plates should have a high electrical and thermal conductivity. It should also be impermeable to gases, mechanically durable, and chemically stable in fuel cell conditions, and it should be cheap and well suited for high-volume manufacturing. The technical requirements for a bipolar plate material, apart from the suitability for manufacturing, are well satisfied by graphite, when its natural porosity is blocked with resin impregnation or other suitable treatment. It is commonly used in the construction of prototype cells and stacks. The flow field plates used in the experimental work of this thesis were made of graphite, with the exception of the cathode plate of the current distribution measurement system.

The main disadvantages of graphite are high cost and poor suitability for cheap manufacturing methods, and therefore, alternative materials are being developed. The most promising flow field plate materials for mass-manufactured fuel cell products are usually considered to be either composites of carbon and polymers [17-21], or metallic materials combined with a suitable surface treatment to reduce corrosion and improve electrical contact [22-27]. Extensive research and product development is continuing on both approaches. Composite materials promise cheap manufacturing by molding, but achieving good mechanical strength and gas tightness together with high electrical and thermal conductivity is challenging. Steel, on the other hand, is a cheap and mechanically durable material, but the channels are difficult to manufacture into it, and achieving sufficient corrosion resistance can be problematic.

2.2.6 Stack design

The voltages required for practical applications usually exceed the voltage of one unit cell. The voltage requirement of the intended application can be satisfied by constructing a stack, which is a series-connected, mechanically integrated assembly consisting of several unit cells. The basic features of a typical PEMFC stack are illustrated in Figure 4. The flow field plates of the stack, with the exception of those at the ends of the stack, have channels on both of their major surfaces, one being the anode side of a unit cell and the other being the cathode side of the next unit cell. Flow field plates of this type are thus called bipolar plates. A stack consisting of MEAs between bipolar plates has a high power density, and low internal resistance can be reached because electrical connection between the unit cells is formed directly through the bipolar plates. The stack shown in the Figure is of a type in which air is supplied using a compressor or a pump. This is usually an optimal choice for large fuel cell systems. A high-power stack may contain additional features, such as provisions for cooling and gas humidification.

The challenges of constructing stacks include ensuring the effective distribution of reactants to all of the electrodes and the removal of excess water from all parts of the stack, and minimizing voltage and temperature differences between the unit cells. In order to be suited for series production, the design should also be mechanically simple and easy to assemble.

In the design of small fuel cell power sources, simplification of the fuel cell system is a central issue. Especially on the cathode side of the cell, optimal solutions may be radically different from those used in large fuel cells. In small applications, pressurization is generally undesirable because of the parasitic power consumption of the compressor. The use of natural convection or a small fan is likely to be the optimal solution in the lower end of the power range. As a result, the choice of the cathode geometry and stack design for small applications is strongly influenced by the necessity of minimizing the flow resistance.

The channel geometry illustrated in Figure 3 enables the construction of a natural convection stack, in which the electronic connection between the unit cells is provided directly through the bipolar plates. Apart from the geometry of the cathode channels, the resulting stack structure is thus similar to the stack in Figure 4.

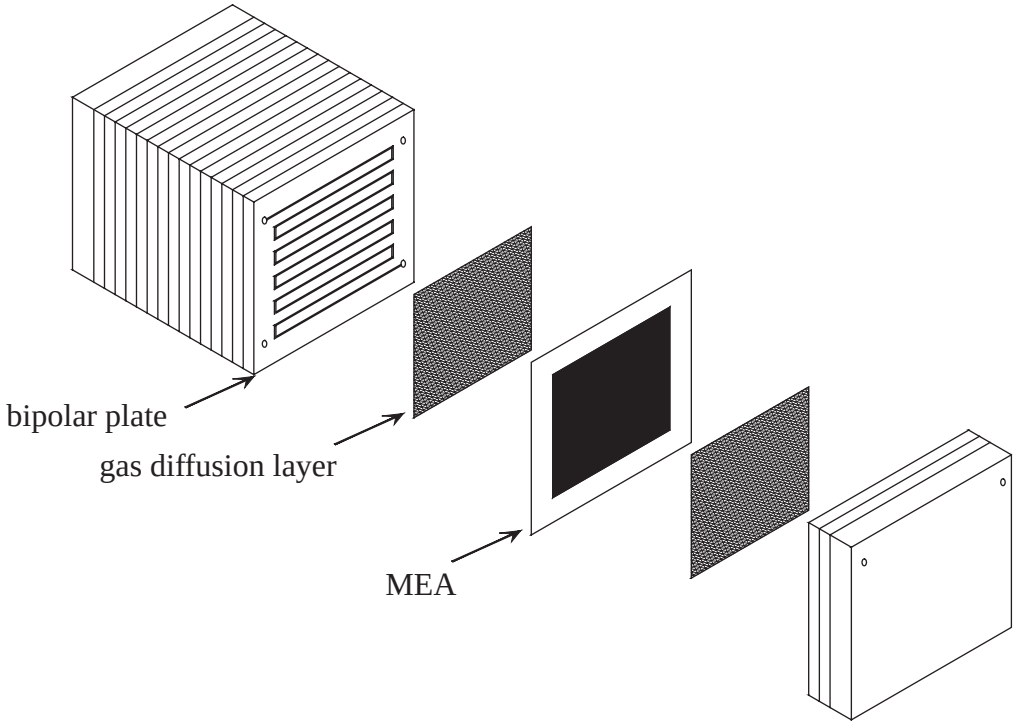

Figure 4. *A PEMFC stack, with exploded view to one unit cell.*

In addition to the geometry used in the present thesis, several different single cell and stack geometries for small fuel cells have been proposed. Some examples include planar cells [28], annular cells [29,30], and strip cell and pseudo-bipolar designs [31-33]. A cell array with "flip-flop" interconnection has also been recently reported [34]. In very small cells, it may be advantageous to utilize silicon substrates and related manufacturing methods [35,36]. Non-traditional stack types usually have the disadvantage of higher ohmic losses resulting from the more complicated interconnections between the unit cells. However, they may be better suited for applications in which there are stringent requirements for the physical form of the cell or where independence of the physical orientation is required.

2.2.7 The polarization curve

The reversible open-circuit voltage of a H_2/O_2 fuel cell at a temperature of 25 °C and pressure of 1 atm is 1.23 V, assuming that the product water is formed in liquid state. Practical open-circuit voltages are lower because of mixed potentials, which may be due to, for example, impurities in the anode gas or molecular hydrogen diffusing to the cathode. The effect of the latter phenomenon increases when extremely thin membranes are used, as it is usually the case in small fuel cells. The open-circuit potential depends on the activities of the reactants, and therefore, it is lower when air is used on the cathode instead of pure oxygen. As a result of these phenomena, the practical open-circuit voltages of PEMFCs are typically in the range of 0.90 ± 0.05 V.

When current is drawn from the cell, various efficiency losses begin to arise. The term "overpotential", which originates from electrolysis cells, is often used for the losses,

although in the case of a fuel cell the effect of the losses is the reduction of operating voltage. The overpotentials in fuel cells are commonly classified to three types, which are

- activation overpotentials, arising from reaction kinetics
- ohmic losses, arising from the resistances of the cell materials and interfaces
- mass transport overpotentials, arising from the limitations of mass transport.

The polarization curve of a PEMFC usually consists of three distinct regions, which result from the three types of overpotentials. The typical shape of the polarization curve is shown in Figure 5. It is important to realize that the curve in the Figure describes only the relation between the average current density and cell voltage. However, significant variation of local current density over the active area is possible, and current distribution measurement is thus an important tool for analyzing local conditions inside the cell.

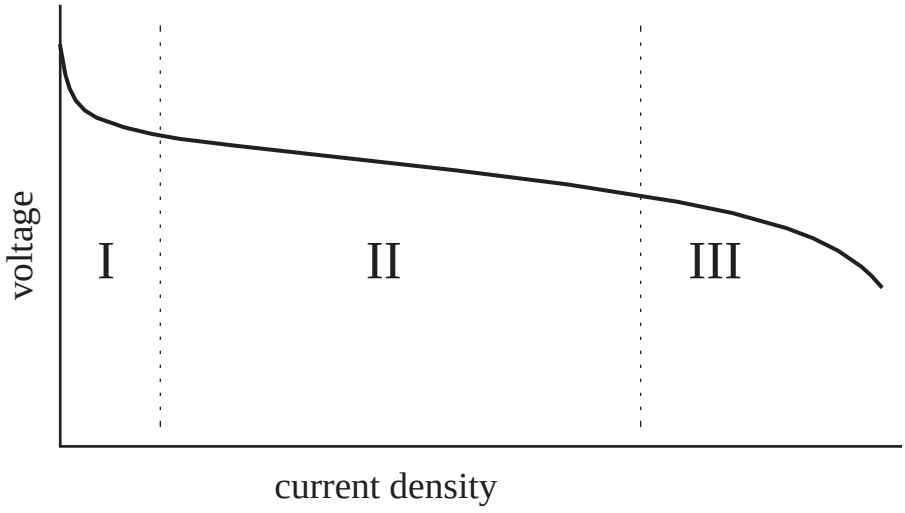

Figure 5. *The typical polarization curve of a PEMFC. The regions dominated by different overpotentials are indicated:*
I activation overpotentials
II ohmic (IR) losses
III mass transport overpotentials.

The achievable current density range covered by the polarization curve depends strongly on operating conditions, and the choice of cell materials and design. High-power cells with pressurized air cathodes, operating near the upper limit of the allowable temperature range, can produce more than 1 A cm^{-2} at practical operating voltages, whereas in small free-breathing cells operating close to the ambient temperature, it may be difficult to exceed 100 mA cm^{-2}.

At low current densities, the shape of the curve is primarily determined by activation overpotentials, which give it the characteristic logarithmic shape. The main source of activation overpotential is the cathode. When pure hydrogen is used as fuel and the cell is well humidified, the activation losses of the anode electrode are negligible. This is caused by the rate of the hydrogen oxidation reaction, which is orders of magnitude higher than the rate of the cathode reaction.

When current density increases, the shape of the curve becomes approximately linear, which reflects the effect of ohmic losses. The membrane is a major source of ohmic

losses, but also the electronically conducting components and the interfaces between the components contribute to them. The dependency of ohmic losses on current density may deviate from linear if the conductivity of the membrane changes as a result of changes in humidity or temperature.

When current density is increased further, the curve begins to bend down, which results from limitations in the availability of reactants at the catalyst surfaces, *i.e.* from the mass transport overpotentials. In addition, mass transport overpotentials contribute to the linear shape of the curve in the middle region. The main source of losses is the cathode side, because the diffusivity of oxygen is significantly lower than that of hydrogen, due to the larger molecule size of oxygen. In addition, flooding problems that cause mass transport limitations are more likely to be encountered on the cathode side, because water is produced there.

The concentration of oxygen that reaches the catalyst surface depends on the concentration gradients arising in the gas channels, the gas diffusion layer, and in the porous electrode. In the gas channels, mass transport is driven by a combination of diffusion and either free or forced convection, depending on cell design. In the gas diffusion layer and in the electrode, gas-phase transport normally takes place mainly by diffusion, except in some special types of cell designs in which the gas mixture is forced into the porous material [37]. The magnitude of mass transport by diffusion depends on the diffusivities of the species, the interaction between the porous medium and the diffusing species, and the interdiffusion effects between different species present in the system.

Several experimental studies have been carried out to explain the effect of mass transport phenomena on the polarization behavior and to identify the losses associated with each cell component. In particular, many studies have concentrated on discerning the losses in the porous electrodes and in the gas diffusion layers from each other. In a review that summarizes the results of several research efforts, Mosdale & Srinivasan [38] state that their experimental results could be explained by interpreting transport limitations in the electrode as the main source of mass transport overpotentials. However, they also note the possibly large effect of losses in the gas diffusion layer in case its porosity is reduced, for example as a result of flooding. The porosity of the gas diffusion layer is also affected by the compression force between the cell components. Lee *et al.* [39] examined the effect of the compression force and found that the amount of compression affected strongly the limiting current density, and it was observable already at the linear region. The limiting current density has been found to be determined by losses in both the catalyst layer and the gas diffusion layer [40], and it is determined more by the mole fraction than the partial pressure of oxygen. For this reason, pressurization of the cell does not significantly increase the limiting current density, although performance at intermediate current densities is improved [41]. The effect of pressure on cell performance is not elaborated further in this thesis, because the focus of the work is on small, ambient-pressure fuel cells.

The losses caused by interdiffusion of oxygen in a mixture of nitrogen and water vapor have been observed experimentally by AC impedance measurements [42], and by the use of different synthetic gas mixtures [43]. The effect of interdiffusion effects is, however, relatively small, especially when the operating pressure is low.

The concentration gradients arising along the length of the gas channels can be expected to depend on the stoichiometries of the gas streams, and the distribution of current across the active area. Current distribution determines the spatial distribution of

the consumption of reactants and the production of water. Because gas composition in turn affects current density, theses factors are interrelated. Moreover, in a natural convection cell, the air stoichiometry is affected by gas composition, because the strength of natural convection depends on density changes in the gas mixture. The factors affecting mass transport in a natural convection PEMFC are thus interrelated in a complex way.

Because the small thickness of the cell components makes direct measurements of local conditions inside the cell difficult, modeling approaches are often used to improve understanding of mass transport in fuel cells. A considerable number of numerical models have been reported for investigating mass transport phenomena in fuel cells. These will be reviewed in Chapter 3.6. In addition, the dependency of the limiting current on operating parameters and cell structure has been studied by analytical modeling [44-46].

2.2.8 Efficiency

Because a fuel cell is not a heat engine, its efficiency is not limited by the Carnot law, which states the maximum efficiency of a heat engine operating between given temperature levels of upper and lower heat reservoirs. Another reason why fuel cells are highly efficient is because energy conversion takes place by electrochemical reactions instead of chemical combustion, which is a highly irreversible process. The latter fact is often overlooked in the discussion of efficiencies, as pointed out by Haynes [47].

The reversible efficiency of a fuel cell is the Gibbs energy change ΔG in the reaction divided by the enthalpy change ΔH in the reaction:

$$\eta_{\text{rev}} = \frac{\Delta G}{\Delta H} \tag{1}$$

The Gibbs energy change in the reaction is related to temperature by:

$$\Delta G = \Delta H - T\Delta S \tag{2}$$

where ΔS is the entropy change in the reaction. In a PEMFC, the available Gibbs energy decreases as a function of temperature, and therefore, the theoretical maximum efficiency decreases slightly as a function of temperature. Because of improved kinetics and mass transport, however, an increase in temperature is generally advantageous for the performance of a PEMFC, within the limits dictated by water management.

The efficiency of a fuel cell is related to the shape of its current-voltage curve. The voltage efficiency of a fuel cell is defined as the relation of cell voltage to the reversible voltage:

$$\eta_V = \frac{E}{E_{\text{rev}}} \tag{3}$$

Any improvement of the cell that results in a reduction of overpotentials obviously brings a direct efficiency gain at a given current density. Another important consequence of Equation (3) is that voltage efficiency decreases with increasing current density.

The current efficiency is defined as the ratio of hydrogen consumed in the anode reaction, obtained from Faraday's law, to the total hydrogen flow fed into the cell:

$$\eta_I = \frac{jA}{2F\dot{n}_{\mathrm{H2}}} \tag{4}$$

where j is current density, A is the active area of the cell, F is Faraday's constant, and $\dot{n}_{\mathrm{H2}}$ is the molar flow rate of hydrogen. Evidently, a high hydrogen utilization rate is desirable from the point of view of achieving maximum efficiency. Ideally, the cell would be operated on 100 % hydrogen utilization, *i.e.* on a stoichiometry of 1. This is also referred to as "dead-end" operating mode. From the system point of view, dead-end operation can be accomplished by either closing the hydrogen outlet of the cell or recirculating the excess hydrogen back to the inlet. In systems in which hydrogen utilization is below 100 %, a typical solution is to combust the excess hydrogen in an afterburner in order to recover its energy in the form of heat, and for safety reasons. However, neither a recirculation system nor an afterburner is easily implemented in a small system, and therefore, it is desirable to operate the cell itself in dead-end mode.

The parasitic losses resulting from power consumption of auxiliary devices must also be accounted for when the efficiency of practical fuel cell system is determined. These losses can be described with the system efficiency η_{S}. In small-scale systems, the parasitic power consumption of auxiliary devices tends to be significant compared to the output power of the cell, which makes it particularly important to simplify the system as much as possible.

The total efficiency of a fuel cell system is the product of the three efficiency components:

$$\eta_{\mathrm{tot}} = \eta_V \eta_I \eta_{\mathrm{S}} \tag{5}$$

Current and system efficiencies usually improve with increasing current density, whereas voltage efficiency decreases. Because of the combined effect of the efficiency components, the peak of the efficiency curve is generally located somewhere between zero and peak power. The nominal efficiency of a fuel cell power system, therefore, depends on the choice of nominal operating voltage. A better efficiency can be reached at the expense of power density at nominal operating voltage, or vice versa. In terms of cost, lowering the operating voltage decreases the cost of the cell per nominal power but increases the fuel cost due to lower efficiency. Conversely, lower fuel cost can be attained by accepting a higher cost per nominal power. This relates the choice of the operating voltage to economic issues.

2.2.9 Water management

Water management in a PEMFC is one of the most essential issues for obtaining good and reliable performance. The commonly used perfluorosulfonate membranes need to be hydrated in order to be proton conductive, and because of the proton conducting phase present in the electrodes, they also need to be humidified in order to function. In other parts of the cell, the amount of liquid water should be kept to the minimum. Liquid water must be prevented from accumulating on the electrode surfaces, in the pores of the gas diffusion layers, and in the gas channels. Liquid water in these regions obstructs the transport of reactants to the active catalyst sites, thus reducing performance. The objective of effective water management is thus to regulate the

transport of water in such way that a sufficient amount of water is retained in the proton conductive phases, but excess liquid water is removed from the cell at the same rate as it is produced, with minimum obstruction of the gas transport paths.

Figure 6 illustrates the flows of water in a PEMFC. Water is produced on the cathode, and additional water may be supplied to the cell along the inlet gas streams if the product water is not sufficient to maintain the proton conductive phases humidified. When ambient air is used as a source of oxidant, the cathode conditions are affected by ambient temperature and relative humidity. Water transport between the anode and the cathode takes place by three different processes. Protons migrating through the membrane drag water molecules along with them. This phenomenon is referred to as electro-osmotic drag. The magnitude of electro-osmotic drag in polymer membranes has been subject to several experimental studies [48-51]. The formation of a water concentration gradient inside the membrane gives rise to diffusion, which usually counters the electro-osmotic drag and is, therefore, often referred to as "back-diffusion". Furthermore, if there is a pressure difference across the membrane, hydraulic permeation contributes to the water transport. The net water transport through the membrane is the resultant of these three processes.

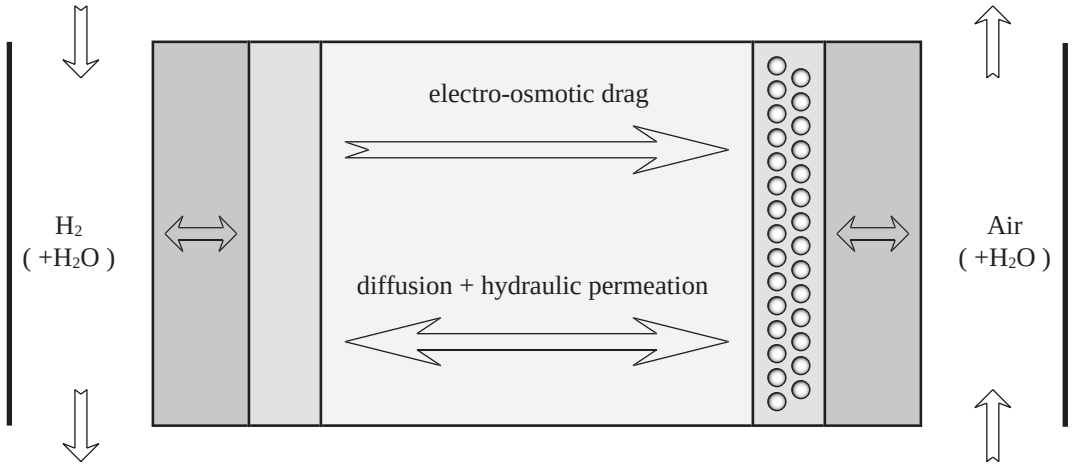

Figure 6. *The flows of water in a PEMFC.*

The net water transport is commonly characterized using the net water transport coefficient α, which is defined as the average number of water molecules dragged by one proton to the direction of the cathode. The direction and magnitude of net water transport is a function of several factors, such as current density, temperature, gas flow rates, and the materials and geometry of the cell. In addition, the value of α may vary across the active area of the cell. It is likely that at high current densities, the electro-osmotic drag dominates, whereas at lower current densities, the back-diffusion process is also significant, and the pattern of net water transport is more complicated and difficult to predict. The fluxes of water between the membrane and the gas streams depend on the local water content in the membrane, and the temperatures, flow rates and gas compositions on both sides of the cell. They are also affected by the properties of the gas diffusion layer. The transport of water in vapor phase takes place through diffusion and convection, similarly as the transport of reactant gases.

In this thesis, the focus is on operating the cell on dry hydrogen, because the use of external gas humidification devices is undesirable in small applications. Inspection of the water streams in Figure 6 reveals that operating the cell on dry anode gas requires

the average value of α, weighted with the current distribution, to be zero or negative. A negative value of α means that part of the product water exits through the anode outlet. If dry hydrogen is used and the anode is operated in dead-end mode, the weighted average of α must be exactly zero, in order to achieve steady-state operation.

2.2.10 Heat management

Operating temperature affects the performance of the cell in several ways. The rates of the electrochemical reactions depend on temperature, the protonic conductivity of membrane materials increases with increasing temperature, and the tolerance of the catalysts against impurities is improved along with it. Increasing temperature also facilitates water removal, thereby enabling higher currents to be drawn from the cell before the onset of flooding. Because the saturation pressure of water increases strongly with increasing temperature, more water transport can take place in vapor form, which is generally more practical than removing water in liquid form. In addition, an increase in temperature increases the diffusivities of gases. If the flow of air on the cathode is driven by natural convection, the flow rate increases with increasing temperature difference to the surroundings.

The temperature of a fuel cell is determined by the balance between its waste heat production and the rate of heat removal. Because of the high power densities characteristic of this fuel cell type, large fuel cells require active cooling, which also enables active temperature control. Active cooling can be arranged using fan-driven air cooling, or in the case of a stack with high power density, using heat exchangers and a liquid heat transfer medium such as water. In laboratory-scale work on single cells and small stacks, external heating is normally used to maintain the cell at its desired operating temperature.

Because of the beneficial effects of increasing temperature, it is generally desirable to operate a PEMFC close to the point where drying problems begin to emerge. It must be remembered, however, that the production of heat occurs within a small space in the electrode, and therefore, the volumetric power density of heat production can be high. Therefore, local heat transfer limitations may give rise to hot spots, which cause drying problems or even material damage, even if the average cell temperature is within allowable limits. Adequate heat removal from the electrode to the surrounding cell structure is, therefore, an important issue in cell design and in the choice of materials, especially when high current densities are sought. In addition, the requirements of portable applications may set limits to the allowable temperature at the exterior surfaces of the cell.

Because of its operating temperature range, the PEMFC is commonly regarded as the most suitable fuel cell type for applications in which the energy supply is primarily required in the form of electricity. The waste heat of a PEMFC is of limited use because of its low temperature. It may be useful for space heating in the immediate vicinity of the cell, but low-temperature heat is difficult to transfer over extended distances. The low temperature of waste heat may also make cooling problematic when high power densities are sought, because the small temperature difference in relation to the environment requires large heat exchanger surfaces to be used.

In small fuel cells, the thermal power density may be relatively small, and active temperature control systems are also undesirable, because extreme system

simplification is sought. Therefore, small fuel cells often need to be operated at relatively low and variable temperatures. Because of the significant effects of temperature on cell performance, variable temperature makes it challenging to achieve good and reliable performance.

2.3 Other fuel cell types

Fuel cells are commonly classified according to the type of electrolyte. Fuel cell types other than the PEMFC are briefly covered here. A more thorough review can be found for example in [52].

Substantial research efforts are being devoted to the development of high-temperature fuel cells, the main types of which are the solid oxide fuel cell (SOFC) and the molten carbonate fuel cell (MCFC). Their applications are envisaged mainly in stationary power production. In addition to the PEMFC, the most important low temperature fuel cell types are the phosphoric acid fuel cell (PAFC) and the alkaline fuel cell (AFC). PAFCs are being sold by a few companies, and some hundreds of units are in field operation worldwide.

A fuel cell type known as the direct methanol fuel cell (DMFC) can be considered a sub-type of the PEMFC. The main difference is the anode reaction, in which methanol is oxidized instead of hydrogen. The electrochemical oxidation reaction of methanol is more complicated than the oxidation reaction of hydrogen, resulting in higher activation overpotentials, and the power density per electrode area is accordingly smaller. However, the rest of the fuel cell system is simplified, which may result in a higher power density for the system as a whole. Most importantly, fuel storage becomes considerably easier because methanol is liquid at room temperature, whereas hydrogen is a gas. The DMFC may be particularly well suited for small applications because of the difficulty of storing hydrogen in a small package. Also, the auxiliary devices needed for hydrogen handling may not be readily available.

The practical differences between the cell types include the types of catalysts and membranes used. In a DMFC, alloy catalysts are necessary to improve the tolerance of catalysts against the CO formed as a by-product of the anode reaction. The membrane of a DMFC should have a minimal permeability for methanol, in order to avoid efficiency losses as a result of lost fuel, and mixed potentials on the cathode. Developing suitable membrane materials is currently regarded as the main issue in DMFC development.

In this thesis, no work on methanol as fuel was done. However, because of the similarities between the fuel cell types, the results of this work also have relevance for the development of DMFCs. From the point of view of optimizing the cathode of the cell, the main difference to hydrogen fueled cells is that more water will be dragged from the anode to the cathode, making flooding problems more severe.

3 Methods

3.1 The fuel cell test station

In all of the experimental work presented in this thesis, a GlobeTech GT-100 Fuel Cell Test Station (GlobeTech, Inc., later on incorporated into ElectroChem, Inc.) was used as the foundation of the measurement system. It was complemented with various auxiliary measurement systems and devices, according to the specific needs of different stages of the work. The test station consists of a gas sub-system, a load unit, and a computer, which performs the tasks of system control and data collection. The principal parts of the test station, and the gas tubes and electrical connections between them, are described in Figure 7.

The gas handling unit feeds the fuel and oxidant gases to the fuel cell. The gases are stored in pressurized bottles. Flow rate is regulated using MKS Type 1179A Mass-Flo® Controllers (MKS Instruments, Inc.). The gases can be humidified in the built-in humidification bottles, in which the gases bubble through water which is maintained at a constant temperature. The gases pick up humidity from the water, and the level of humidification can be controlled by adjusting the temperature of the bottles. The humidification bottles can be bypassed if dry reactant gases are desired. In the experiments reported in this thesis, only the anode part of the gas-handling system was used in most of the measurements, because the test cells had open cathodes, into which air was fed using natural convection or a fan. An exception to this was the characterization of the sinter material, which was done using a small single cell with forced oxygen supply. The gas handling unit also contains back-pressure regulators, which can be used to control the gas pressure in the cell. Pressurization, however, was not used in any of the measurements of this thesis.

The load is a Scribner Series 890 Fuel Cell Load Unit (Scribner Associates, Inc.). It is air-cooled and rated at 100 W. It can be controlled in galvanostatic (constant current) or potentiostatic (constant voltage) mode, or in constant power mode. Galvanostatic control was used in all of the measurements, because water production is directly proportional to current density, and consequently, constant current leads to constant rate of water production, which facilitates water management. The load unit features a built-in current interrupter circuitry, which can be used to measure the ohmic resistance of a fuel cell. The current interruption method will be discussed in Chapter 3.2. Integrated in the load unit, there is also a temperature control sub-system, which can be used to control the temperature of the cell. This sub-system consists of a thermocouple sensor, two heating cartridges, and a temperature controller.

The computer that controls the measurement systems runs a FuelCell® software (Scribner Associates, Inc.) with a variety of system control, data acquisition, and display features. The computer communicates with the load unit via GPIB, and the load unit transmits the control signals to the gas handling unit.

The procedures and practices in the use of the equipment in the experimental work were based on experience gained from the previous experimental work of our group. It has been described in detail in references [53-56].

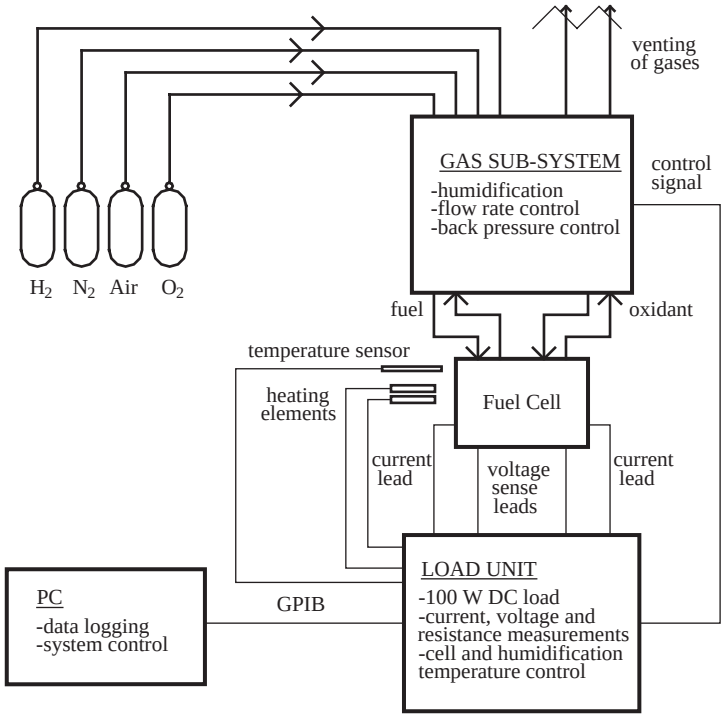

Figure 7. *The fuel cell test station used in the work of this thesis.*

3.2 The current interruption method

The measurement of ohmic losses is an important practical tool in the analysis of water management in a PEMFC because changes in the hydration state of the membrane are directly reflected in the resistance of the cell. The measurement of ohmic loss in a fuel cell is not straightforward because it has to be separated from the contributions of other overpotentials. In addition, the ohmic loss results from the resistances of both the proton conductive and the electronically conductive components of the cell. However, it can usually be assumed that if the compression forces between the cell components remain constant, any short-term changes in the resistance of the cell result from changes of the membrane resistance.

In this thesis, the current interruption method was used for the measurement of ohmic losses. The method is also known as the current step method. The use of different variations of this method to measure the ohmic loss in electrochemical cells has been described in [57-60]. The current interruption method is based on the use of rapid current transients to separate the different overpotentials from each other. The practical implementation of the method involves the use of either a fast switch to interrupt the current or a separate circuitry to feed a current pulse into the cell. The latter approach has been found to yield more accurate results, especially when current is high [59,60]. The required high speed of the switch and the low impedance of the circuitry are difficult to attain when the circuitry should be able to carry a high current. In the test station used in this work, the current interrupter circuitry was of the genuine interrupter type. Because relatively low total currents were used, this was regarded as sufficient.

The current interruption method takes advantage of the nearly instantaneous disappearance of ohmic losses when a rapid current transient occurs. In a PEMFC, the decay of the ohmic losses to less than 1 % of the initial value has been estimated to take place within 0.5 ns of the interruption [59]. Electrochemical losses, on the other hand, respond with considerably longer time scales. For the fastest decaying part of the electrochemical losses, the same authors mention an experimentally obtained time scale of 10 ns.

Figure 8 illustrates the shape of a voltage transient when current is interrupted and subsequently switched on again. In the case of a current pulse, the shape of the transient would be inverted. From the Figure, it is evident that the ohmic loss can be measured by recording the voltage of the cell immediately before and immediately after the interruption. Ideally, the difference between the recorded voltages should represent the ohmic loss. The practical implementation of the method is more complicated because of the impedances of the measurement circuitry and the noise of the electronics. An example of a real voltage transient is illustrated in Figure 9. The signal contains noise from the measurement electronics, and a voltage overshoot is observed immediately after the interruption.

In practical measurement setups, some of the decay of the electrochemical losses in the cell occurs already before the overshoot and subsequent oscillations have fully subsided. This has been reported to occur even in specialized measurements systems with an extremely low inductance [59]. Therefore, the shape of the voltage transient needs to be extrapolated back to the moment of interruption, in order to obtain the true *IR*-free voltage. Otherwise, some of the fastest decaying electrochemical losses would be misinterpreted as ohmic loss.

The current interrupter system of GT-100 test station performs the data collection and processing internally and produces the final reading to the computer screen and to the data files. While this is often sufficient when the method is used for routine monitoring of the cell, some important additional insights can be gained by observing the entire voltage transient. This can be done, for example, using a digital oscilloscope or other rapid voltage sampling device. Recording the entire transient makes it possible to assess the quality of the data and to perform extrapolations when they are needed. Because the oscilloscope probes can be freely attached to any part of the measurement circuitry, it can also be used to detect sources of error resulting from the non-idealities of the circuitry. For example, in preliminary measurements it was found that in the GT-100 system, the resistance reading given by the software that controls the measurement system is systematically overestimated [55]. Additional investigations revealed that the resistance of one of the current leads is included in the reading, which causes the error [56].

Using only single measurements for the calculation of the ohmic loss may also lead to a decrease of data quality when the cell voltage is unstable. Consider a case where the cell voltage is rising or falling when the current is interrupted. Between the measurement of the initial voltage level, and the interruption, some change of voltage takes place. When the ohmic loss is calculated, this change would erroneously be included in the ohmic loss reading. This can be avoided by visualizing the entire voltage transient to obtain the precise voltage at the moment of interruption.

The ohmic loss of a fuel cell can also be obtained using impedance spectroscopy [42,61-63]. It is based on observing the response of the cell to AC signals by simultaneous voltage and phase measurements. Impedance spectroscopy can be used to

obtain also other information than the magnitude of the ohmic loss. However, when one is mainly interested in the ohmic loss, the current interruption method provides the needed information with good accuracy and relatively straightforward data analysis.

In Publication V, the current interruption method was used to measure the ohmic losses in individual cells of a stack. From practical experience on stacks it is known that large variations of cell voltage may exist among different unit cells of the stack. Therefore, it is important to investigate reasons for the observed voltage differences and to discover methods to achieve a more uniform voltage profile. The key to attaining these goals is to separate the contributions of different overpotentials from each other in each unit cell. The measurement of only the polarization curves of unit cells, combined with good understanding of electrochemistry, may lead to qualitatively correct interpretations of the performance limiting factors in different unit cells. However, the direct measurement of ohmic losses will always reduce the need for guesswork and thereby provide a more firm basis for the search of performance gains.

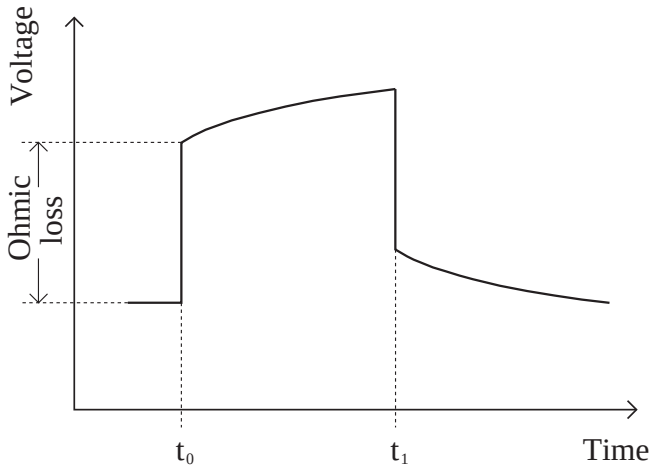

Figure 8. *The principle of the current interruption method.*

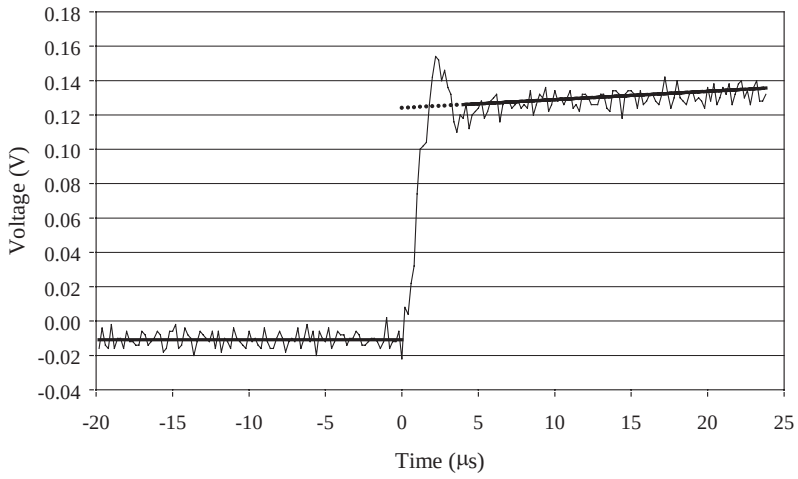

Figure 9. *A measured voltage transient after a current interruption in a fuel cell. The zero of the voltage scale corresponds to average cell voltage.*

3.3 Current distribution measurement

Local current density can vary considerably over the active area of a fuel cell. Therefore, significant performance gains may be achievable by discovering ways of taking more effective use of the active area. In this thesis, current distributions in a free-breathing cell were studied experimentally, using a segmented current collector plate. This is the first implementation of a current distribution measurement system in the context of a free-breathing cell. The construction and test measurements with the cell are described in Publication I. The same measurement system was utilized in Publications II, III and IV to obtain parameters for modeling work, to perform water transport measurements, and to investigate the effect of environmental conditions on cell performance.

Current distribution measurements in PEMFCs have received growing interest in recent years. A number of different approaches have been reported for this purpose. The measurement system used in this thesis is based on the use of a segmented current collector. Current is collected by electrically conductive segments, which are embedded in a supporting structure made of a non-conductive material. Current is measured from each segment individually, and a mapping of current distribution as a function of position on the active area is obtained. Other segmented cell designs have been reported by several groups [64-70].

An alternative method is the use of Hall-sensors, which are embedded in the flow field plate [71]. In addition, a segmented cell in which current distribution is measured with Hall-sensors has been reported [72].

The segmented cathode current collector plate used in this work is illustrated in Figure 10. The channel geometry of the plate consists of parallel straight channels, with their ends open to the outside air. The cross-sectional dimensions of the channels are 3 x 3 mm. The dimensions of the active area are 50 x 50 mm. The resolution of the segment matrix is 12 segments in the horizontal and 4 segments in the vertical direction. On the anode side of the cell, a non-segmented graphite plate was used.

Because the segments need to be isolated from each other and they must be individually adjustable, small air gaps exist between the segments in the same rib of the flow field, as seen in Figure 10. For this reason, the geometry does not consist of strictly separate parallel channels. However, the variation of cell performance and mass transport conditions is likely to be more significant in the along-the-channel direction, and therefore, the slight equilibration of gas composition through the small air gaps is not expected to severely distort the results.

The segmentation is not extended into the gas diffusion layer and the electrode. Because an electrical contact among the segments exists through the gas diffusion layer, it is important to quantify the magnitude of error resulting from this. In Publication I, results of simulation work are presented to obtain insight into current flow in the gas diffusion layer.

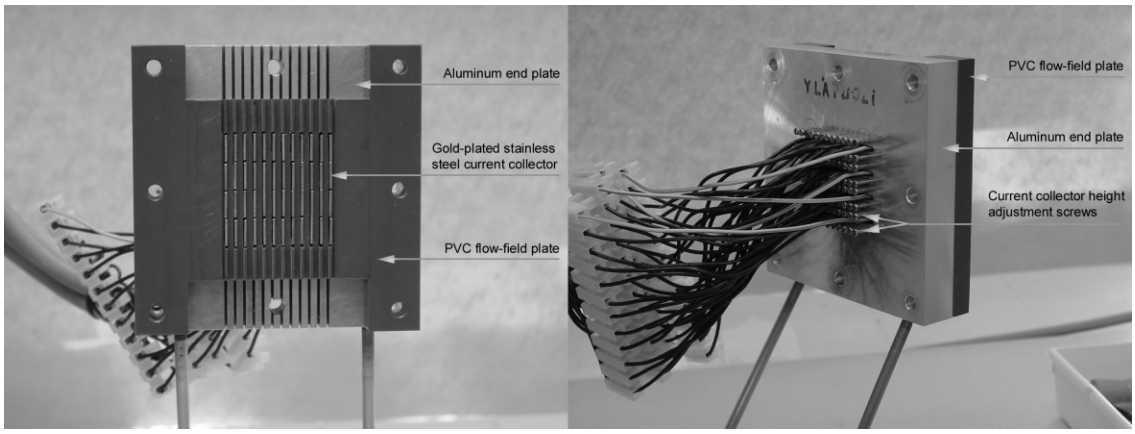

Figure 10. *The segmented current collector plate.*

Because only the flow field is segmented, it is essential that all of the segments are in good contact with the gas diffusion layer in order to obtain reliable results. To achieve this, the measurement plate is equipped with individual adjustment screws for the pressure of each current collector segment against the gas diffusion layer. The massive supporting structure of the plate also helps to ascertain good contact for all of the segments, because it prevents the structure from bending when the retaining bolts are tightened.

Before the measurements, the segments were carefully leveled. The leveling was verified by operating the cell at low (< 50 mA cm^{-2}) current density and measuring the voltage drops through each current path. At low current densities, significant mass-transport related differences in local current density are not expected to occur. When significant local deviations from the average current density level were observed, they were corrected by adjusting the screws.

A separate data logging system was used to record the current densities. The scanning of the entire segment matrix took approximately 2 seconds. The measured voltage drops were converted to current densities using the assumption that each segment collects current from an equal area.

3.4 Water transport measurements

The net water transport through the membrane significantly influences the overall water balance of the cell, and it was thus considered an important issue to be investigated experimentally. The measurements are described in detail in Publication III. The segmented cathode plate was used in the measurements, and a water collection arrangement was added to the measurement setup. Several previously published studies on water transport in PEMFCs exist (*e.g.* [73,74]), but small fuel cells operating on dry gases at ambient pressure and low temperature have so far received little attention. The only previously published study on water balance in a natural convection cell focused on a different cell geometry [28]. In addition, water collection measurements have not before been combined with the measurement of current distribution.

Water collection was performed by allowing the gas exiting the anode side of the cell to flow through a glass tube, in which moisture was captured from it using a drying agent. Water was collected from the anode side outlet, because in a natural convection cell, it

would be difficult to connect a water collection tube to the cathode channels without disturbing the air flow. A $CaSO_4$-based Drierite® drying agent (W.A. Hammond Drierite Co. Ltd.) was selected because it should be effective for capturing moisture even from gas with a low partial pressure of water. The tube leading from the anode outlet of the cell to the drying tube was heated in order to prevent the condensation of water in the tube. The amount of collected water was determined by weighing the drying agent before and after the measurement. In addition to collecting water, simultaneous measurements of cell polarization, resistance, and current distribution were performed.

The rate of water production in the cathode reaction can be calculated using Faraday's law:

$$\dot{n}_{\mathrm{H2O}} = \frac{jA}{2F} \tag{6}$$

When the water production rate given by Equation (6) is multiplied by the duration of the measurement, the amount of water produced is obtained. Making the reasonable assumption that the collected water originates entirely from the cathode reaction, the percentage of water exiting through the anode can then be calculated from the ratio of the collected water to the total water production.

Net water transport can alternatively be expressed as the net water transport coefficient α, which gives the number of water molecules transported through the membrane per proton, as discussed in Chapter 2.2.9. It is known that two protons must be transported through the membrane for one water molecule to be formed in the cathode reaction. By using this information, the coefficient α can be calculated from the measurement data. The result should be interpreted as the average of α over the active area, weighted with the current distribution.

An alternative approach for the extraction of water from a gas would be cooling the gas to a low temperature, such as in [28] and [74]. When the experimental setup for the work of Publication III was being developed, some tentative experiments were made with a measurement setup in which the anode outlet gas was led through a vessel enclosed in an ice bath. However, the approach that uses a drying agent proved easier to implement using available equipment, and therefore, the ice bath approach was abandoned.

3.5 Climate chamber measurements

The temperature and relative humidity of the ambient air can be expected to affect the performance of a free-breathing cell. The effect of these factors was thus seen as an important topic to be studied experimentally. For this purpose, a measurement setup was constructed in a climate chamber (ArcTest Oy), in which temperature and relative humidity could be controlled. The experiments were performed using the current distribution measurement system, which was placed in the chamber inside a protective box in order to shield it from the effect of air currents caused by the air circulation system of the chamber. The measurement of current distribution is a new feature compared to previous climate chamber studies reported in the literature [31,75,76].

The test station described in Chapter 3.1 was used also in these measurements, with some simplifications resulting from practical considerations. Active temperature control

was not used, and therefore, the cell temperature was determined by the balance between heat production in the cell and heat removal to the surroundings. In addition, resistance measurement could not be performed due to the inductances of the long current cables needed. Publication IV describes the work in more detail.

3.6 Modeling

Modeling can be used to gain insights into mass transport conditions inside the fuel cell. By modeling, it is possible to provide quantitative predictions on the local values of gas mole fractions and flow velocity, which are difficult to measure directly. Considerable efforts have been devoted to the modeling of fuel cells by several authors. The important early works of Bernardi and Verbrugge [77,78], and Springer *et al.* [41,79] were one-dimensional descriptions of the central parts of the cell. The original Bernardi and Verbrugge model has later been improved [80]. The models of Fuller and Newman [81], and Nguyen and White [82] include simplified descriptions of two-dimensional phenomena, and true two-dimensional models have later been reported by several authors [83-91]. Three-dimensional models have also been recently reported [92-94], and some groups have included two-phase transport [87-93,95,96], non-isothermal effects [82,92,93,95,97], and dynamic behavior [84,88,96]. However, all of the above mentioned models describe cells with forced air feed. The only theoretical study on free-breathing cells is by Li *et al.* [16], who developed analytical equations for the prediction of the current-voltage behavior.

In the present work, a numerical model of mass transport on the cathode side of the cell was developed in order to quantify the local mole fractions of oxygen and water vapor, and flow velocity. Some main features of the model are reviewed here, and a more detailed description of the model can be found in Publication II. The model describes a cathode gas channel and gas diffusion layer in two dimensions. The model is steady-state, isothermal, and describes gas-phase transport. The main new aspect of the model is the description of buoyancy as the driving force of mass transport. The model was implemented using the FEMLAB® multiphysics package (COMSOL AB), which runs within the MATLAB® environment (The MathWorks, Inc.). The calculations were performed on an SGI Origin 2000 computer system (Silicon Graphics, Inc.).

Special emphasis had to be placed on the treatment of flow resistance in the channel. In the modeling of a natural convection cell, the flow velocity cannot be prescribed as an input parameter. Instead, it will be determined as an output variable of the model, from the balance between the driving forces and the flow resistance. This necessitates some improvement to a two-dimensional model. Normally, a two-dimensional model assumes the model region to extend to infinity to the direction normal to the model plane. However, the real shape of the flow channel is a rectangular pipe, and a conventional two-dimensional model thus considerably underestimates its flow resistance, because two of the walls are unaccounted for. A more realistic description can be created by the method of volume averaging, which means the integration of the flow profile of the missing dimension into the two-dimensional model. A more extensive discussion on the use of volume averaging in fuel cell modeling can be found in [98].

In the model developed in the present work, the components of the volume averaged Navier-Stokes equation take the form

$$\frac{6\rho}{5}\left(\frac{\partial\langle u\rangle^2}{\partial x}+\frac{\partial\langle u\rangle\langle v\rangle}{\partial y}\right)=\mu\left(\frac{\partial^2\langle u\rangle}{\partial x^2}+\frac{\partial^2\langle u\rangle}{\partial y^2}\right)-\nabla p-g(\rho-\rho_0)-\frac{\mu\langle u\rangle}{B^2/3}$$

$$\frac{6\rho}{5}\left(\frac{\partial\langle u\rangle\langle v\rangle}{\partial x}+\frac{\partial\langle v\rangle^2}{\partial y}\right)=\mu\left(\frac{\partial^2\langle v\rangle}{\partial x^2}+\frac{\partial^2\langle v\rangle}{\partial y^2}\right)-\nabla p-g(\rho-\rho_0)-\frac{\mu\langle v\rangle}{B^2/3}. \qquad (7)$$

where ρ is density, x and y are model coordinates, $\langle u\rangle$ and $\langle v\rangle$ are the respective volume-averaged velocity components, p is pressure, g is the acceleration of gravity, μ is dynamic viscosity, and B is the half-width of the channel. The subscript 0 refers to ambient conditions. The features resulting from the volume averaging are the last terms of the equations and the 6/5-factors on the left hand sides of the equations. Buoyancy is described by the second last terms of the equations. The Navier-Stokes equation is solved only in the channel region.

The mole fraction of component i in the gas channel is solved from the equation:

$$\mathbf{N}_\mathrm{i}=-D_\mathrm{i}\nabla X_\mathrm{i}+X_\mathrm{i}c\langle\mathbf{u}\rangle \qquad (8)$$

where $\mathbf{N}_\mathrm{i}$ is molar flux, D_i is diffusion coefficient, X_i is mole fraction, c is total concentration, and $\langle\mathbf{u}\rangle$ is volume-averaged velocity vector. In the gas diffusion layer the fluxes are described by the Stefan-Maxwell equation:

$$\nabla X_\mathrm{i}=\frac{1}{cD_\mathrm{ij}}\sum_\mathrm{i}(X_\mathrm{i}\mathbf{N}_\mathrm{j}-X_\mathrm{j}\mathbf{N}_\mathrm{i}) \qquad (9)$$

where D_ij is the interdiffusion coefficient between components i and j. The cathode electrode is included in the model as a boundary condition. Measured current distributions are used to define the fluxes of oxygen and water vapor at this boundary:

$$\mathbf{n}\cdot\mathbf{N}_\mathrm{O}\big|_{x=0}=-\frac{\mathbf{n}\cdot\mathbf{j}(y)}{4F}, \qquad \mathbf{n}\cdot\mathbf{N}_\mathrm{W}\big|_{x=0}=\frac{\mathbf{n}\cdot(1+2\alpha)\mathbf{j}(y)}{2F} \qquad (10)$$

where $\mathbf{n}$ is normal vector at the boundary. The use of a measured current distribution enables the calculation of the local oxygen consumption and water production without modeling the membrane and the anode side of the cell. The value of the net water transport coefficient α, however, still needs to be either assumed or measured. From the discussion on water transport in Chapter 2.2.9, it is evident that the theoretical prediction of α would require a full-cell model, which was outside the scope of the present thesis.

During the model development, the possibility of extending the model to the third dimension was investigated. With a true three-dimensional model, it would be possible to make predictions on mass transport conditions in the regions of the gas diffusion layer adjacent to the ribs of the flow field. Because the transport path between these regions and the gas channel is longer, it is likely that oxygen mole fractions in these regions are lower and water mole fractions higher than those predicted by the present model. However, it became apparent that the memory requirements of a true three-dimensional model were beyond the capabilities of the Matlab-based modeling environment, and therefore, it was decided to use the two-dimensional approach with a

volume-averaged description of the channel region. A two-dimensional model should be able to produce reasonable approximations of mass transport conditions in most of the gas diffusion layer volume of the modeled cell, because the width of the flow channels is three times the width of the ribs.

4 Results

4.1 Current distribution measurements

The first experiments with the current distribution measurement system aimed at the determination of the accuracy and reliability of the measurement system. The gas diffusion layer and the electrode were not segmented, and this can be assumed to lead to some degree of smoothing of the current distribution. Furthermore, local variability in the contact pressure of the pins against the gas diffusion layer can be expected to distort the results, and therefore, it is essential to minimize the variability.

In order to minimize the differences in contact pressures, the flow field was carefully leveled before the measurements, using the adjustment screw system described in Chapter 3.3. The results indicate that the leveling was generally well accomplished. In most cases, some sporadic non-idealities remained, but their effect was small and easily distinguished from mass transport related effects. As an example, Figure 11 (a) depicts a case in which two of the segments ((6,1) and (8,1)) had a better contact to the gas diffusion layer than the surrounding segments, resulting in an upward deviation from the overall shape of the distribution, and slight downward deviations in the surrounding segments. This is caused by the tendency of electric current to seek the path with the lowest resistance. In addition, the deformation of the gas diffusion layer as a result of excess pressure at one segment may cause a weaker contact at the surrounding segments, which further reduces their readings. However, as seen in the Figure, the deviations are small compared to the variability caused by other effects.

Examples of the effect of a segment with a weak contact to the gas diffusion layer can be found in Publication IV. A segment with a poor contact appears in the current distribution mapping as a small local depression, with the surrounding segments deviating upward from the overall shape of the distribution.

Excessive contact pressure can also cause increased resistance to mass transport in the gas diffusion layer, resulting in a real reduction of local current density at the electrode. However, with most gas diffusion layer types, excessive contact pressure can be detected afterward by inspecting the gas diffusion layer for unusually deep depressions.

As a result of the experiments, it can thus be concluded that when the contact pressure of an individual pin against the gas diffusion layer is either weak or excessive, the effect can be in both cases easily identified by examining the distribution data and the cell. Therefore, the risk of misinterpreting non-idealities in the data as being the result of mass transport phenomena is small. The magnitude of the distortions appears to be tolerable, and it does not influence the overall form of the distribution.

The largest uncertainty exists with regard to the corner segments, where the effect contact pressure variations may not be easily distinguished from mass transport effects. In the corners, it is more difficult to determine, whether the obtained value deviates from the overall shape. In the measured current distributions, it was frequently observed that local current densities at the corner segments deviated downward from the overall shape of the distribution. This can be seen for example in the distribution in Figure 11 (a). The effect of contact resistance variation cannot be completely ruled out, but it appears more likely that this is mainly due to lower temperature, and mass

transport related effects. The channels at the edges of the flow field are narrower than the rest of the channels, as seen in Figure 10. This decreases local current density in the corners and elsewhere along the vertical edges of the flow field.

The lack of segmentation in the gas diffusion layer probably does result in some smoothing of the current distribution, even when there is no variability in the contact pressures. A simple model was developed to quantify the magnitude of the error. In Publication I, results are given for a case in which a current density of 150 mA cm^{-2} was assumed under one of the segments and a current density of 300 mA cm^{-2} under the other segments. The difference in the current densities between neighboring segments is rather steep compared with those that are expected to be found when the cell is operated under reasonable conditions. Even in the highly uneven distribution seen in Figure 11 (b), differences significantly higher that this are not encountered. Examination of the model results indicates that the segment under which the current density is lower is collecting current from a slightly enlarged area. However, the enlargement, estimated from Figure 13 in Publication I, is only 15 % even in this rather extreme case, indicating that the smoothing should remain within acceptable limits. Possible additional effects may be caused by the measurement circuitry, and including them in the model may thus be a worthwhile direction for more elaborate theoretical treatment of the problem.

In some publications on current distribution measurements, methods have been proposed for reducing the smoothing effect of lateral currents. The methods include extending the segmentation into the gas diffusion layer and the electrode [64], and using an array of several individually controlled loads to maintain the segments at the same potential [66]. However, the authors of these publications do not mention having attempted to quantify the actual benefit of these methods, and therefore, some uncertainty remains over the issue.

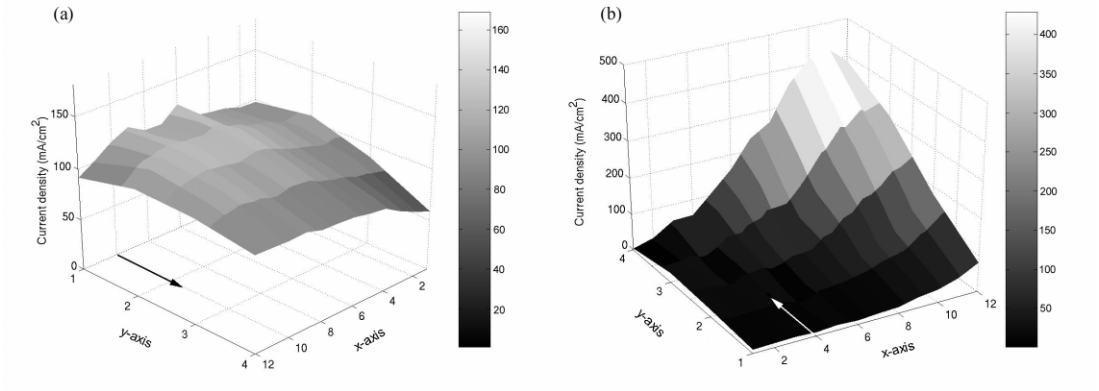

Figure 11. *Example results from current distribution measurements, representing nearly uniform (a) and highly non-uniform (b) distributions.*

As an overall conclusion from the preceding discussion, it can thus be stated that the data obtained with the current distribution measurement system can be considered to represent the true current distribution of the cell with a sufficient accuracy and reliability. However, the data and the cell should always be inspected closely for indications of contact pressure variations, and the probable slight smoothing of the distribution should be taken into account when distributions with steep local variability are measured.

The segmented current collector plate was used in Publications I to IV. The measurements covered a current density range up to 300 mA cm^{-2}, a cell temperature range up to 75 °C, and a range of ambient temperatures from 10 to 40 °C. In the majority of the experiments, the cell was operated in the orientation shown in Figure 10, *i.e.* the channels oriented vertically. In the measurements reported in Publication II, some experiments were made on operating the cell with the channels oriented horizontally. Significant accumulation of liquid water in the channels was observed, and average current densities higher than 40 mA cm^{-2} could not be obtained. It was thus concluded that the channel geometry is not suited for operating in this orientation. In the measurements of Publication I, a sheet of paper enfolded around the top of the cell was used to strengthen the air flow caused by natural convection. It was found to improve performance, but it was not adopted as a standard practice due to concerns on the reproducibility of the geometry.

The measured current distributions exhibited significant variations as a function of current density, cell temperature, anode conditions, and ambient temperature and humidity. In Publication I, one of the objectives of the study was to determine the feasible operating temperature range of the cell. It was found that good performance was obtained at 60 °C, but above this temperature, drying problems began to emerge. At 75 °C, most of the cell area was found to be nearly inactive, as seen in Figure 11 (b). On the basis of these observations, cell temperatures above 60 °C were excluded from the subsequent measurements.

The drying of the membrane phase was detected using the current interruption method. In most of the measurements, the ohmic loss readings were obtained using the software of the measurement station. As discussed in Chapter 3.2, this results in less accurate readings than analyzing the voltage transients with an oscilloscope. The readings given by the test station are slightly overestimated, and random scatter is increased when the cell voltage is unstable. The latter phenomenon was observed, for example, in the measurements reported in Publication I. However, for the purposes of most of the experimental work, the accuracy obtained using the built-in features of the test station was considered acceptable.

In Publication I, some tentative conclusions on oxygen transport and flooding phenomena were made. However, the exact nature of mass transport phenomena cannot always be reliably deduced from the current distribution data itself. Therefore, other experimental techniques and modeling were used to complement the current distribution measurements. These will be discussed in the next sub-chapters.

4.2 Modeling

Modeling was used to obtain insights into mass transport in the cathode channels and gas diffusion layer. The modeled cases represented cell temperatures of 40 and 60 °C. The current densities were 100 and 200 mA cm^{-2} at 40 °C, and 100, 200, and 300 mA cm^{-2} at 60 °C. Measurements were performed with the current distribution measurement system at these temperature and current density levels to obtain current distributions to be used as boundary conditions. Cell voltage and resistance were measured simultaneously with the current distributions.

In the experimentally obtained current distributions, the local current density was generally decreasing toward the upper end of the channel, especially at high current densities and at the lower temperature level. It was also found that, at the highest current density levels, the cell voltage decreased slowly with time and exhibited increasing short-term fluctuations. The cases corresponding to the highest current density levels can thus not be classified as genuinely steady-state. However, it was regarded as justified to include them in the calculations, in order to create a wide range of cases for modeling. When evaluating the stability of cell voltage, it should also be remembered that the magnitude of short-term fluctuations of voltage in natural convection cells is generally higher than in cells operating on forced convection.

Example results for the mole fractions of oxygen and water are given in Figures 12 and 13. The rest of the results are given in Publication II. The results quite strongly indicate that the cell operated in a partially flooded state when the cell temperature was 40 °C. The relative humidities at the upper end of the channel were above 100 % at both current density levels. At the cell temperature of 60 °C, the experimentally obtained performance was improved compared to the lower temperature level. According to the model results, this can be partly attributed to a higher flow rate, which enables more effective removal of water and more even distribution of oxygen to the electrode. The model results for flow velocity are 0.013 - 0.016 m s^{-1} at 40 °C and 0.022 - 0.025 m s^{-1} at 60 °C. It thus appears that velocity is primarily determined by the temperature difference between the cell and its surroundings. Another factor that contributed to improved performance was the saturation pressure of water vapor. At 60 °C, the saturation pressure is 170 % higher than at 40 °C, and accordingly, the removal of water in vapor state is more effective. Because the model did not indicate flooded conditions, it was concluded that the current distributions in the 60 °C were mainly determined by the availability of oxygen in the channel.

In the base case, the model was solved using an assumed net water transport of α = -0.25. This means that 50 % of the product water is assumed to exit the cell through the anode outlet. Experimenting with different values of α revealed that it affects quite significantly the water mole fraction predicted by the model. When α was varied from -0.4 to -0.1, the predicted maximum of water mole fraction at j_{ave} = 300 mA cm^{-2} and T_{cell} = 60 °C varied by up to 48 % compared to the base case. However, it could be determined that when the value of α was varied, the changes in the model results for velocity and oxygen mole fraction were small or moderate. At j_{ave} = 300 mA cm^{-2} and T_{cell} = 60 °C, the variation compared to the base case result was up to 6 % for the mole fraction of oxygen and up to 12 % for flow velocity. Comparison of the modeling results with the operational stability attained during the experiments indicates that the real value of α was probably less negative than what was assumed. At 60 °C and 300 mA cm^{-2}, experimental cell voltage was found to fluctuate increasingly with time, which is likely to have been caused by flooding. Model results, on the other hand, gave a relative humidity of 82 % at the upper end of the model region, which does not indicate saturation. This suggests that the water mole fraction was probably underestimated.

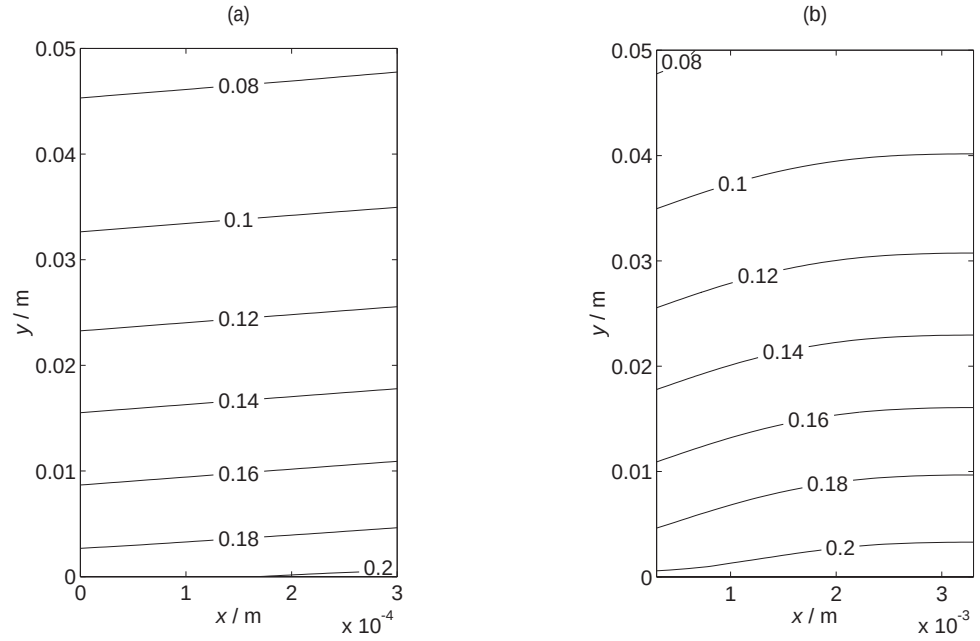

Figure 12. *Model results for the mole fraction of oxygen in the gas diffusion layer (a) and in the gas channel (b). T_{cell} = 60 °C, j_{ave} = 300 mA cm^{-2}.*

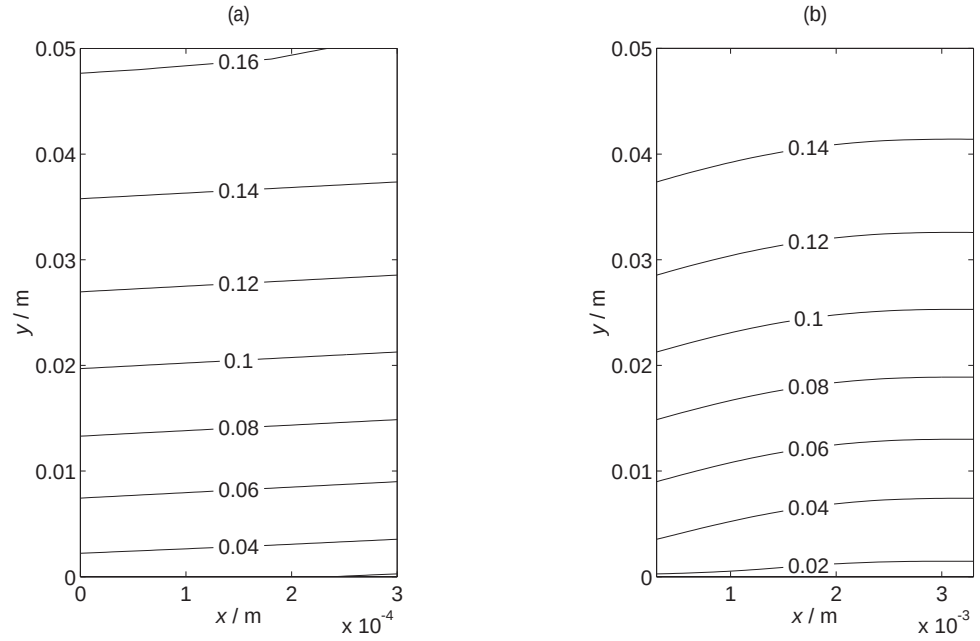

Figure 13. *Model results for the mole fraction of water vapor in the gas diffusion layer (a) and in the gas channel (b). T_{cell} = 60 °C, j_{ave} = 300 mA cm^{-2}.*

When the results from the modeling work are assessed, the assumptions included in the model must be carefully considered, and taken into account when the model is developed further. The development of the model was limited by the memory handling capabilities of the modeling environment, but it can be expected that advances in software development will enable the construction of more elaborate models in the future.

The results quite clearly indicate that most of the time the cell operated at or near saturation conditions, and liquid water was thus likely to exist in the gas diffusion layer. Liquid water is not currently included in the model, which probably results in some overestimation of the porosity of the gas diffusion layer. Furthermore, oxygen mole fractions are artificially reduced in the model results when the saturation limits are exceeded, because this results in overestimated mole fractions of water vapor. Therefore, two-phase modeling should be investigated in the further development of the model. This also emphasizes the need for a better understanding of the interaction between liquid water and the gas diffusion layer.

The model results clearly confirm that temperature strongly affects mass transport conditions inside the cell. Therefore, deviations of the real temperatures from the temperature assumed in the model may impair the reliability of the results. Temperature distribution inside the cell is affected by heat production of the electrodes and the heating elements, and heat transport in the cell materials and between the cell and its surroundings. Relative humidity is probably the most severely affected solution variable because of the steep dependency of saturation pressure on temperature. Flow velocity in the channel should reflect the average temperature along the channel, and consequently, small local deviations probably do not radically compromise the reliability. However, it must be remembered that the cell temperature used in the calculations was a measured value, which was obtained with a single temperature sensor. It is difficult to ascertain how well it represents the average temperatures of the channel walls. The supporting structure of the plate is made of plastic with relatively poor thermal conductivity. Therefore, the existence of significant temperature differences along the length of the channel and even between the channel walls is possible. The magnitude of the temperature dependency of flow velocity can be estimated by comparing the model results for flow velocity at different cell temperatures. When temperature is increased from 40 to 60 °C, flow velocity increases by 70 % at 100 mA cm^{-2} and 44 % at 200 mA cm^{-2}. The treatment of non-isothermal effects is likely to be another worthwhile issue in further developments of the model.

Despite relying partly on experimental data, the model can also be of some help in cell geometry optimization. For example, the examination of the Darcy-type flow resistance term reveals that the flow resistance caused by the channel is strongly dependent on its cross-section. The dimensions of the channel were 3 x 3 mm in all of the studied cases. Increasing the width by only one millimeter (*i.e.* to 4 mm wide and 3 mm deep) would reduce the Darcy-term by more than 40 %. Repeating the model calculation for these channel dimensions, using T_{cell} = 60 °C, α = -0.25, and assuming a constant j = 200 mA cm^{-2} throughout the electrode, results in an increase of 25 % in predicted flow velocity. Alternatively, it might be beneficial to reduce the length of the channels, because the present channel length appears to lead to relatively large variations of water mole fraction along the length of the channels.

4.3 Water transport measurements

Using an assumed value of the net water transport coefficient resulted in some uncertainty in the results of the modeling work. This emphasizes the importance of an experimental study on water transport. The results of water transport measurements are reported in detail in Publication III.

In order to connect the results to the modeling work, the levels of average current density and temperature were chosen to be the same as the steady-state cases in the experimental part of Publication II. These were 100 and 200 mA cm^{-2} at 60 °C, and 100 mA cm^{-2} at 40 °C. To obtain a sufficient resolution in the water collection measurements, the durations of the measurement runs were extended compared to those used in the work of Publication II. The duration was normally 4 hours at each set of measurement parameters, unless high water production required it to be shortened. Using a relatively long measurement time should also help to minimize the distortion of the results by the possible accumulation of water inside the cell. For the same reason, a stabilization period of one hour was used.

Another major aim of the experiments was to investigate the effect of anode conditions on water transport. In a free-breathing cell, the cathode conditions cannot be actively controlled, and consequently, the relative importance of the anode side from the point of view of water management increases. One measurement series was performed with the anode in flow-through mode, using stoichiometry levels of 1.5, 2.0, and 2.5. In addition, the flow direction of hydrogen was varied. Hydrogen entered the cell from either an upper or a lower corner of the flow field, resulting in the general flow direction of either down or up, respectively. These different anode conditions can be expected to affect the net water transport and the distribution of water inside the cell. In the measurements reported in the other Publications, hydrogen was usually fed through the lower inlet, with the exception of the work of Publication I, in which the upper inlet was used.

The hydrogen stoichiometries used in the flow-through case may appear unrealistically high when considering a single cell only. However, it must be remembered that in stacks it may be useful to design anode manifold geometries in which the anodes of several unit cells are connected in series with respect to gas flow. This may lead to hydrogen stoichiometries which are even higher that those used in the work of Publication III.

The results in the flow-through case indicate that hydrogen stoichiometry affects the net water transport significantly. The percentage of water expelled through the anode increased approximately linearly with increasing stoichiometry. At 40 °C and 100 mA cm^{-2}, the percentage varied between 2 % and 10 % depending on the anode conditions. At 60 °C and 200 mA cm^{-2}, the range of variation was from 2 % to 58 %. At 60 °C and 100 mA cm^{-2}, the cell operated on the threshold of drying, and as a result, steady-state operation could only be achieved when the direction of hydrogen flow was down. The amount of collected water in this case was small. The drying problems and the high percentages of water removal through the anode in some cases at 60 °C can be understood by considering the strong temperature dependency of the saturation pressure of water vapor.

The current distributions recorded during the water collection measurements were found to depend primarily on the average current density, hydrogen flow direction, and cell temperature. The dependency on hydrogen stoichiometry was found to be small in the majority of the cases, with the exception of T_{cell} = 60 °C, j_{ave} = 200 mA cm^{-2}, and upward hydrogen flow direction. The shapes of the distributions can be interpreted by considering the variation of water transport over the active area. When the general direction of hydrogen flow was down, the shapes of the current distributions were considerably more even than when the direction was up, as seen for example in Figure 14. This gives indication of changes in the magnitude and direction of water transport.

When the general direction of hydrogen flow was down, there was a strong water flux from the cathode to the anode in the upper parts of the cell, because hydrogen was dry in the upper parts of the cell, and on the other side, the upper parts of the cathode were operating close to saturation. Toward the lower edge of the active area, the situation changed and the magnitude of water transport toward the anode decreased, and even a reversal of direction may have occurred. The outcome was the redistribution of water from the upper parts of the cell, which were operating close to saturation, to the lower parts, which were operating close to dehydration. On the other hand, when the direction of hydrogen flow was up, this redistribution of water did not take place. Dry hydrogen caused severe drying in the lower parts, and moisture picked up by the hydrogen in the upper parts simply exited the cell without being redistributed to other parts. Indications of drying near the hydrogen inlet can also be found in the data reported in Publications I and IV.

The conclusions are supported by the inspection of cell polarization and resistance measurements. In the cases where the hydrogen flow direction was down, cell resistance was generally lower and voltage higher than when the direction was up. This results from the favorable effect of water redistribution in the cases where the flow direction was down. Again, the dependency on stoichiometry was small, with the exception of the case T_{cell} = 60 °C, j_{ave} = 200 mA cm^{-2}, and hydrogen flow direction up, in which the cell was operating on the threshold of drying.

As an important general observation on the results, it can be concluded that the variation of α across the active area must be considered for the accurate determination of water transport. The combination of measurement techniques used in Publication III helps to draw qualitative conclusions on the local variation of α, even if it does not yield the exact local values of the coefficient. More direct measurement of local water transport phenomena has been reported to be possible, but it requires highly sophisticated methods such as neutron imaging [99].

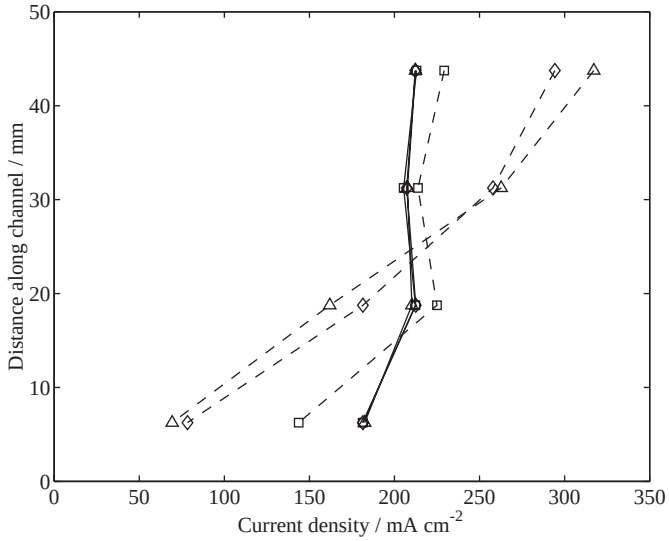

Figure 14. *Current distributions averaged in the horizontal direction. Stoichiometries of hydrogen 1.5 (□), 2.0 (◊) and 2.5 (Δ), general directions of hydrogen flow up (– –) and down (—). T_{cell} = 60 °C, j_{ave} = 200 mA cm^{-2}.*

The results from the water transport measurements can also be used to complement the conclusions of the modeling work of Publication II. In the modeling study, a value of α = -0.25 was assumed. However, measurement data from Publication III indicates that when the cell temperature was 60 °C and hydrogen was flowing down at a stoichiometry of 1.5, the weighted average of α was very close to zero. According to the sensitivity analysis carried out in Publication II, the assumption of α = -0.1 resulted in a water mole fraction of 0.225. This exceeds the saturation limit, which is 0.198 at this temperature. Therefore, it appears likely that in the modeled cases, the cell was operating under flooded conditions at least at the highest current density level at 60 °C, and the flooding at 40 °C was even more severe than indicated by the model results.

Further measurements were performed with the cell operating in dead-end mode, *i.e.* on a stoichiometric amount of hydrogen. The levels of temperature and current density were the same as in the flow-through series, and the direction of hydrogen flow was varied. Gas tightness of the cell in dead-end mode was checked using leak detection spray (AGA TL4) and an Edwards Gas-Check B4 leak detection device (Edwards High Vacuum International, Ltd.). Neither of these methods revealed observable leaks in the cell or the connectors of the gas tubes, and it was thus concluded that essentially all of the hydrogen fed into the cell was consumed in the anode reaction.

The results indicate that, despite the lower flow rates of hydrogen, the anode conditions significantly affected the current distribution, cell voltage, and resistance, although the dependencies were less clear than in the flow-through case. Drying problems were slightly less severe than in the flow-through case, due to the absence of water removal through the anode. In some cases, contrary to the previous series, hydrogen flow direction up resulted in better performance, at least when cell voltage is used as a measure of performance. This may indicate that the cell was operating close to the limit of flooding, and performance was thus improved by increased water removal when hydrogen flow direction was up. However, a case in which water is evenly distributed in the cell may still represent a more optimal situation, even if a lower voltage is observed in a short-term measurement, because an uneven distribution of water may lead to the formation of local dry spots and reduced lifetime of the cell.

Operation in dead-end mode was found to be steady-state over the measurement period of 4 hours in all of the cases. In long-term operation, the possible effect of the accumulation of water and inert gases in the anode channels should be investigated. In sustained operation, it may turn out be necessary to periodically purge the anode side in order to maintain steady-state operation.

It is also interesting to note that in most of the measurements in both flow-through and dead-end mode, current density was increasing toward the upper end of the channel, contrary to most of the current distributions presented in the other Publications of this thesis. The likely reason is that the measurements were performed in the middle of the winter, and the outside temperature was exceptionally low. This resulted in a lower room temperature and lower relative humidity than in the measurements of the other Publications. Water vapor pressure in the air entering the cell was thus low, which resulted in more drying conditions inside the cell. Therefore, there was less flooding in the upper parts of the cell, and on the other hand, there were drying problems in the lower parts. The ambient temperature, averaged over both of the measurement series, was 21 ºC, and the average relative humidity was 15 %. For comparison, during the experiments of Publication II, the ambient temperature was 28 ºC and relative humidity

was 46 %. Calculation of the respective vapor pressures reveals that in the latter case, the water vapor pressure is more than seven times as high as in the former case.

4.4 Climate chamber measurements

Further insight into the effect of ambient conditions on cell performance can be found by inspecting the results of the measurements performed in the climate chamber. The temperature and relative humidity in the chamber were controlled, whereas the cell temperature was allowed to change freely. The chamber temperature range was from 10 to 40 °C, and a relative humidity range up to 90 % was covered.

The highest temperature differences between the cell and the air in the chamber were obtained at the lowest chamber temperature (10 °C). The highest limiting current densities were also obtained in this case. This observation is in agreement with the modeling results, which indicate that the air flow rate is primarily determined by the temperature difference between the cell and its surroundings. When the chamber temperature was increased, this generally led to a reduction in the temperature difference, and accordingly, to a lower limiting current. An increase of cell temperature should allow more water to be transported in vapor form, but the benefit of this appears to have been offset by the reduction in air flow rate. A slight deviation from the decreasing trend in limiting currents can be observed by comparing Figures 3 (a) and (b) in Publication IV. At T_{amb} = 40 °C, the limiting currents were slightly higher than at T_{amb} = 30 °C. However, inspection of the temperature readings in Table 2 of the same Publication reveals that the temperature difference between the cell and its surroundings was slightly higher at T_{amb} = 40 °C, and the result is thus consistent with the interpretation that the limiting current under the studied conditions was mainly dependent on the air flow rate, which is determined by the temperature difference.

Inspection of current distributions provides more detailed information on flooding at the upper end of the current density range. It appears that highly uneven current distributions usually occurred in the region of the polarization curve that was dominated by mass transport limitations. The effect of relative humidity on flooding behavior was found to increase with increasing temperature. The effect of relative humidity was clearly seen in the current distributions from a measurement series in which the ambient temperature was maintained at 40 °C and the humidity of the air in the chamber was varied. The current distributions show that when the humidity of ambient air was increased, the flooded region expanded toward the lower end of the channels. Changes in oxygen partial pressure in the channels were not sufficient to explain the changes in the current distribution. The extreme ends of the series are depicted in Figure 15, and the complete series is shown in Publication IV.

Cell resistance data is not available from the climate chamber measurements, but comparison of the linear parts of the polarization curves in the Publication indicates that significant changes in resistance did not occur. Resistance measurements described in the other Publications also indicate that drying is generally not expected to be a problem within this temperature range. However, possible slight local drying is observable in the segment (4,12) in the Figure, probably resulting from the drying effect of dry hydrogen near the inlet of the hydrogen channels. The drying effect is limited to a small area near the inlet, because the mole fraction of water vapor is high

on the cathode side, resulting in rapid humidification of the hydrogen by water transported through the membrane. This interpretation is in agreement with the results of the water transport measurements discussed in Chapter 4.3.

In order to improve cell performance in situations in which the cell temperature and the temperature difference between the cell and the surroundings are low, it may be worthwhile to consider methods for removing the excess water partly in liquid form. This could be achieved, for example, by methods that rely on capillary action. Water removal in liquid form would not be affected by the rate of air flow or the partial pressure of water vapor in the cathode channel.

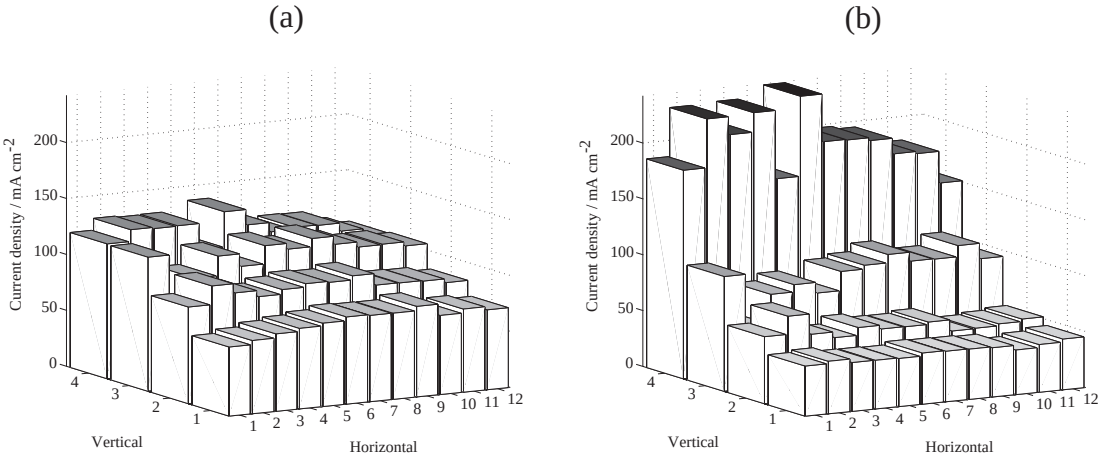

Figure 15. *The effect of the relative humidity of ambient air on flooding. Low humidity (a) and high humidity (b) cases are shown.*

4.5 Measurement of the ohmic losses of individual cells in a stack

The current interruption method is a commonly used measurement technique for the determination of ohmic losses in fuel cells. However, the application of this method to the measurement of ohmic loss of an individual cell in a stack has not been discussed in literature. The subject is briefly mentioned in an older publication [100], but no results are given.

Publication V discusses the application of the current interruption method to the direct measurement of ohmic losses in individual cells of a stack. The work reported in the Publication derives from initial work by Mikkola, reported in [56]. In the work of Mikkola, the possibility of separating the ohmic losses in different unit cells from each other was demonstrated. In addition, the sources of error present in the measurement setup were explored and the typical time scales of transient phenomena during a current interruption were determined. In the present work, the measurement method was improved to allow for faster and more accurate measurements, and a successful measurement series was demonstrated.

The measurements reported in Publication V were performed using a small commercial stack which consisted of four unit cells, seen in Figure 16. The active area of the stack

was 25 cm^2 per unit cell, and the channel geometry was similar to that of the current distribution measurement plate. The stack was not opened or modified in any way to prepare it for the measurements. Current interruptions were produced with the built-in current interrupter circuitry, and the oscilloscope was connected in parallel with the unit cell being measured.

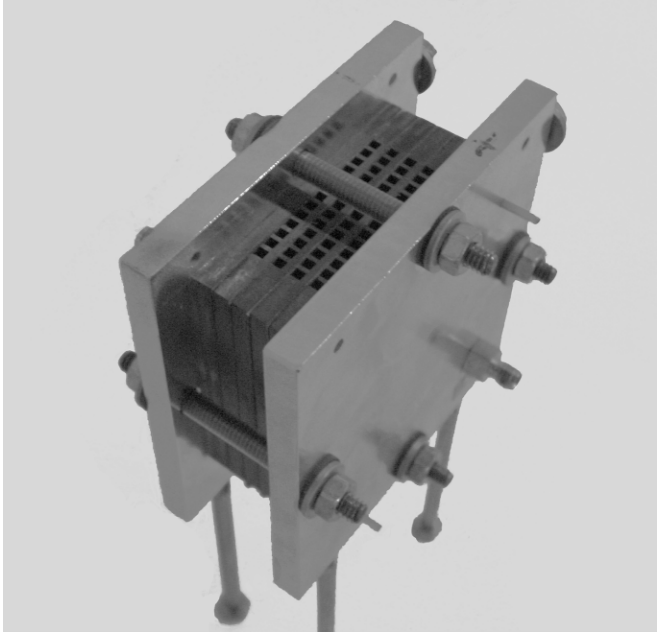

Figure 16. *The four-cell stack used in the experiments of Publication V.*

As an important practical observation, it was found that the oscilloscope must be isolated from the ground in order to take a reading with a single measurement without disturbing the operation of the stack. The stack was grounded through the measurement system, and therefore, a voltage measurement device connected to the stack must be disconnected from the ground. If a grounded measurement device is connected to one of the unit cells, a parallel current path to ground is formed, distorting the results severely. The problem caused by grounding can alternatively be solved by taking two measurements from each unit cell, one from the anode side plate and one from the cathode side plate, both referenced to the end of the stack, and subtracting the anode reading from the cathode reading. This approach was used in the work of Mikkola. In this approach, it is not necessary to disconnect the oscilloscope from the ground. The disadvantage of this approach is the longer measurement time, which results from the need to take two readings for each unit cell. This increases errors resulting from short-term changes in the ohmic losses.

During the measurements, the stack was operated on both natural and forced convection. This enabled a wide range of different water management conditions to be created. No external temperature control was used, because it was regarded as worthwhile to investigate the performance of the stack under realistic operating conditions. Forced convection was provided with a small fan, which was installed in a cardboard housing under the stack and directed toward the channel inlets. Some of the air moved by the fan also flowed past the end plates of the stack, providing external cooling.

Examination of the recorded voltage transients indicates that the duration of the overshoot and the oscillations after the interruption was approximately 3-4 μs. Recalling the time scales discussed in Chapter 3.2, it is evident that the main concern in the analysis of the results was to avoid interpreting the fastest decaying part of the electrochemical losses as ohmic. The ohmic loss was obtained from the recorded transients by linear extrapolation back to the moment of current interruption. The real shape of the voltage transient would probably be more closely described by exponential fitting as in [59]. However, because of the amount of noise present in the data and the relatively small number of data points in the possible nonlinear region, reliable fitting by nonlinear methods was not possible. Therefore, linear fitting was used to obtain consistent results. The correction resulting from the extrapolation was small, of the order of a few millivolts. It appears that the accuracy of the results cannot be improved by the use of more elaborate extrapolation methods. A measurement circuitry with a lower inductance would be needed to shorten the duration of the non-idealities at the beginning of the transients.

Comparison of the ohmic losses and unit cell voltages reveals that the reliance on unit cell voltage measurements may lead to erroneous conclusions on the performance limiting processes in a stack. Figures 17 and 18 depict the outcome of the measurements in the forced convection case. Figure 17 shows that when current density was increased, an increase of cell resistance took place in the middle cells (2 and 3), compared with the unit cells at the ends of the stack (1 and 4). The increase was up to 21 % at 400 mA cm^{-2}, compared with the unit cell with the lowest ohmic loss. However, the profile of the unit cell voltages in Figure 18 is markedly different. The highest unit cell voltage was obtained from cell 1, the lowest from cell 4, and the middle cells represent intermediate values. Monitoring the unit cell voltages alone would not have revealed that the middle cells were on the threshold of drying.

The most likely reason for the uneven ohmic loss profile at high current densities is the drying of the middle cells, as a result of an uneven temperature distribution. The verification of this conclusion by direct temperature measurements was not attempted. It would be difficult because of the small volume in which the increase of temperature is likely to happen.

The higher air flow rate in the forced convection case was another factor that contributed to the increase in ohmic losses by increasing evaporation. The ohmic losses at 200 mA cm^{-2} were 47-49 mV per cell on forced convection, whereas on natural convection, readings of 29-32 mV per cell were obtained at the same current density. However, this does not explain the differences observed in the ohmic losses of the unit cells at high current densities, and therefore, an uneven temperature profile remains as the most logical interpretation for the differences between the unit cells.

Because the rise of temperature probably takes place unevenly across the active area, it is possible that practically dead regions existed in the middle cells at high current densities. Therefore, the problem may be more severe than the magnitude of the ohmic losses alone would indicate. Because an increase of resistance also increases heat production, this may lead to the formation of local hot spots and even cause material damage, even if the drying is not widespread. Another reason why the measurement of ohmic loss may actually underestimate the severity of the situation is because the readings are likely to be affected by uneven current distributions. However, the stack was not equipped for current distribution measurement, and therefore, the effect of this factor cannot be quantified.

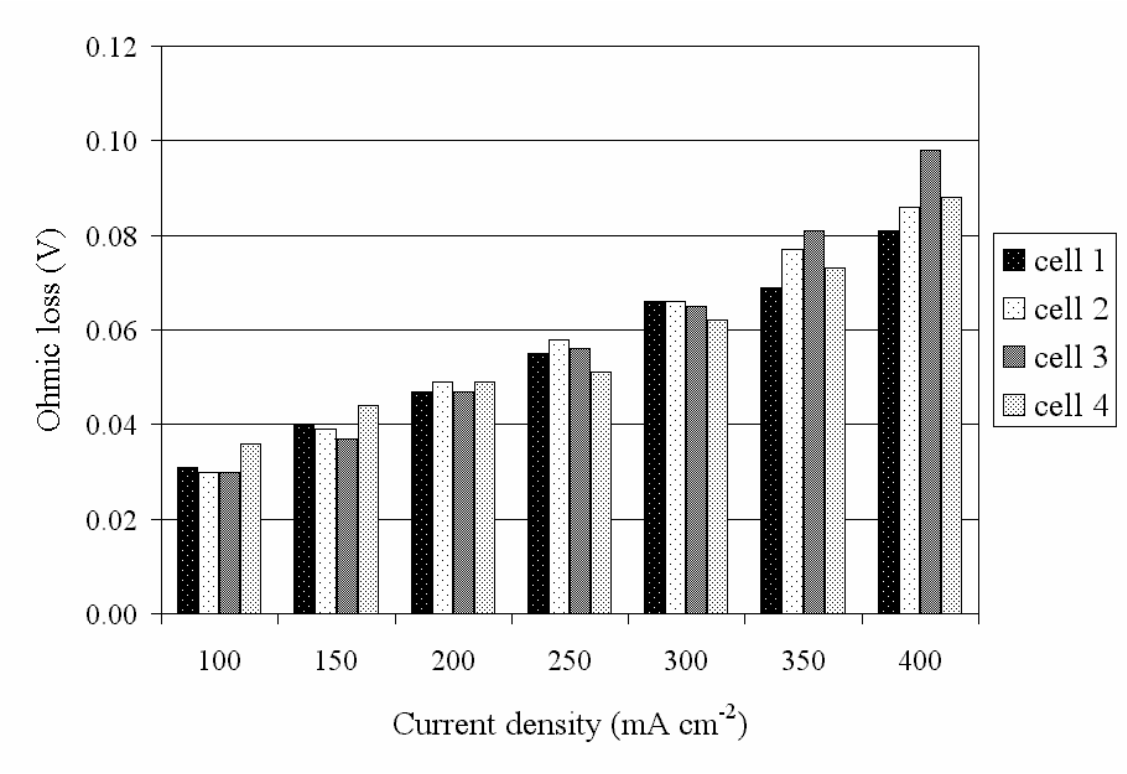

Figure 17. *Ohmic losses in the unit cells of a four-cell stack on forced convection. As current density is increased, an increase of ohmic losses in the middle cells is observed.*

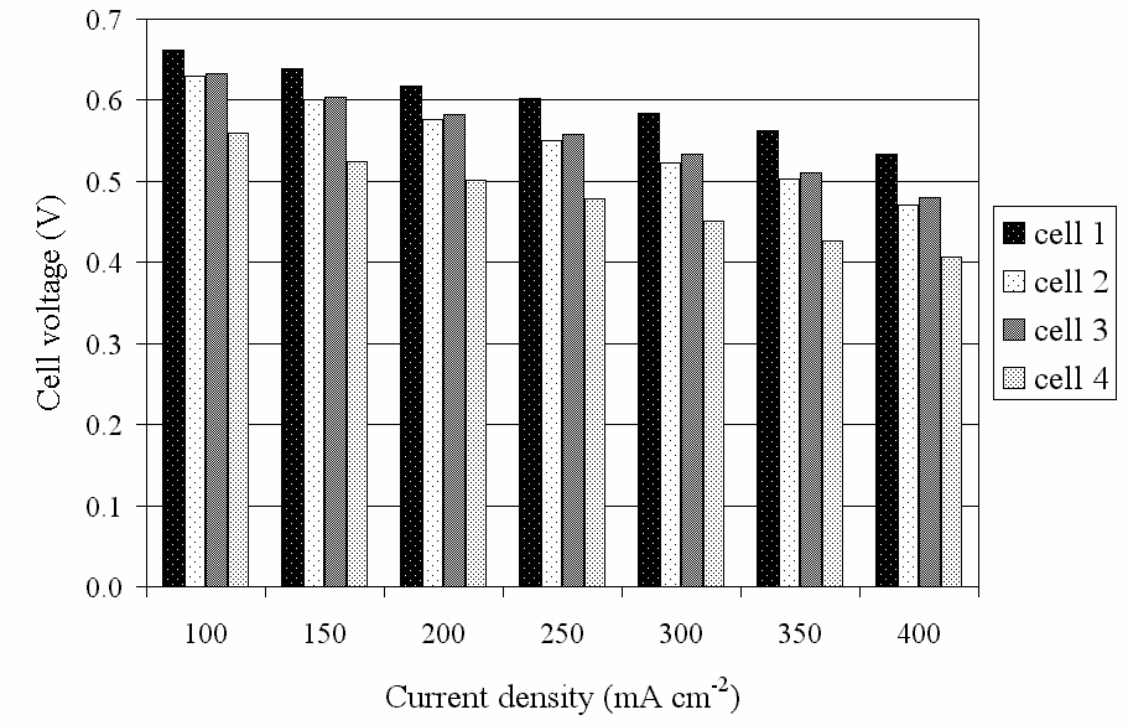

Figure 18. *Unit cell voltages in the unit cells of a four-cell stack on forced convection. Note the difference of the voltage profile compared to the variation of ohmic losses in Figure 17.*

The sum of the obtained ohmic losses in individual cells was in good agreement with the total ohmic loss measured as a single reading for the entire stack. A reading of the ohmic loss of the whole stack was taken before and after the measurement sequence of the unit cells. The total ohmic loss that was calculated from the sum of the individual cell measurements exhibited a smaller amount of random scatter than the readings obtained by a single measurement of the whole stack. A possible reason for this may be found by considering the overshoot after the interruption. When a single measurement of the whole stack is taken, the initial overshoot is large, and the uncertainty in the *IR*-free voltage is accordingly higher.

The observations made as a result of the measurements can be used, for example, to optimize the air feed into the cell. Air stoichiometry was probably quite high in the measurements in which forced convection was used. Decreasing the fan power from the setting used in the measurements might have improved performance, because it would have reduced water removal. However, in some cases this might also lead to drying out, because it would have reduced cooling, resulting in increased evaporation. When a method is available for the measurement of ohmic losses at unit cell level, it becomes easier to determine whether natural or forced convection is the optimal air supply method for a given operating situation, and in the case of forced convection, to optimize the fan power.

4.6 Characterization of sinter materials

The results obtained from the experimental and modeling studies discussed in the previous chapters indicate that in order to achieve effective water removal and oxygen supply on natural convection, it would be advantageous to enlarge the cross-section of the air channels. Increasing the channel width would be the most desirable way of achieving this, because increasing the channel depth would make the unit cell thicker. Increasing the channel width, however, requires improved mechanical rigidity from the gas diffusion material, and therefore, sinters become an interesting alternative to carbon-based materials. The experimental evaluation of a sinter material as gas diffusion layer is detailed in Publication VI. A brief description of the main results is given here.

The studied material was a 0.5 mm thick titanium sinter, supplied by Labgas Instrument Co. In the Publication, a porosity of 55 % was given for the material. However, a later verification of the result with a more accurate method gave a porosity reading of 32 % [101]. Carbon paper, which was SGL CARBON ®SIGRACET BB-10B, was used as a reference material. A reference measurement was performed with a carbon paper on both sides. In subsequent measurements, the carbon paper on either anode or cathode side was replaced with the sinter material.

The main results of the measurements are shown in Figure 19. The data is the same as reported in Publication VI, but the graphs have been redrawn, and the resistance units have been replaced with the more commonly used $m\Omega\ cm^2$. The resistance of the cell with an unmodified sinter was found to be up to seven times as high as in the reference case. A platinum coating was sufficient to bring the total resistance of the cell down to a value that was approximately three times as high as the total resistance using a carbon paper. This confirms the initial assumption that the higher resistance of the cell using

sinters was primarily due to contact resistances and not the bulk resistance of titanium. The thickness of the sinter, therefore, did not significantly affect the comparison with the resistance of the carbon paper.

The results also indicate that the coating slightly improved mass transport on the cathode side, compared with the unmodified sinter. It is possible that the platinum coating made the material more hydrophobic, thus improving the removal of liquid water from the pores. An unmodified sinter is highly hydrophilic, and consequently, water was not expelled from it as effectively as from the carbon paper, resulting in the onset of flooding at a lower current density than with the carbon paper.

In the assessment of the results, it must be remembered that the use of a rigid material makes it possible to increase the ratio of channel width to rib width in the flow field, reducing the effect of flooding of the gas diffusion layer in the regions adjacent to the ribs. In addition, the sinter was slightly thicker than the carbon based material, and therefore, mass transport limitations in the sinter may have been exaggerated in the results. A thinner sinter together with a flow field geometry with wider channels can thus be expected to result in a significantly more favorable comparison against the reference material. Therefore, the present results, despite being promising, do not yet demonstrate the full potential of sinter type materials.

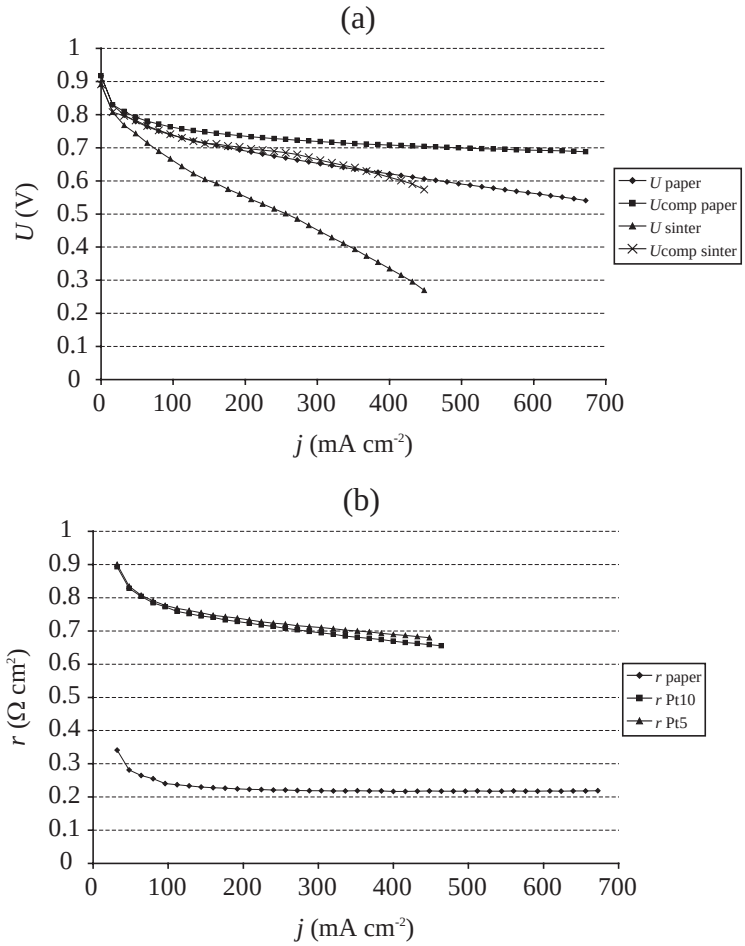

Figure 19. *Polarization curves (a) and area-specific resistances (b) obtained using sinter materials with Pt coatings. A reference measurement with carbon paper is shown for comparison.*

5 Summary

The motivation to this thesis arose from the need to gain a better understanding of mass transport phenomena in a polymer electrolyte membrane fuel cell using natural convection for air supply. The aim was to be able to identify the performance limiting processes and to indicate opportunities for performance improvements. The subject was studied using a variety of experimental and modeling techniques, some of which were novel developments. The work focused on a cathode channel structure consisting of parallel rectangular channels in vertical orientation. The benefits of this geometry include low internal resistance and high power density.

An important theme of the work was to achieve a more effective utilization of the active area of the cell. The basic tool in this work was a current distribution measurement system, which was based on the use of a segmented current collector. As the first phase of the research work, it was considered a priority to ascertain that the measurement system produces reliable and accurate results. The lack of segmentation of the gas diffusion layer and the possibly uneven contact pressures of the collector segments against the gas diffusion layer were identified as the most significant potential sources of error. The results of test measurements indicate that the variation of contact pressures can be reduced to an acceptable level. The effect of the remaining variations can be easily identified in the data as small local deviations, which do not distort the overall form of the current distributions. The error caused by lateral currents in the gas diffusion layer was investigated with a numerical simulation of the current field in the gas diffusion layer and the current collector segments. The results indicate an error of 15 % when an extreme difference in current density between the areas under adjacent collector segments was assumed. In a more typical case, the error should be significantly smaller. Furthermore, the results of the test measurements confirmed the existence of significantly uneven current distributions especially in the direction along the channels. This proved the usefulness of current distribution measurements as the choice of research method.

In order to clarify and quantify the preliminary analysis of mass transport made on the basis of the experimental work, a mass transport model of the cathode side of the cell was developed. The model was constructed to determine the flow velocity and the mole fractions of oxygen and water vapor in a cathode channel and gas diffusion layer. The model was constructed in two dimensions, and the three-dimensional geometry of the channel was accounted for by the method of volume-averaging. This enabled the construction of the model with moderate memory requirements, while still providing a relatively good approximation of the true geometry of the channel. The model made it possible to determine, whether flooding of the gas diffusion layer or insufficient air flow in the channel was the reason for uneven current distributions. In the cases studied with the aid of the model, the limiting current density was found to be determined by flooding, which resulted from insufficient removal of water in vapor form at high current densities. The limiting current density was found to be strongly dependent on the operating temperature of the cell. This was caused both by the effect of temperature on the rate of air flow in the channel and the temperature dependency of the saturation pressure of water vapor. The prediction of water mole fraction in a half-cell model depends on the availability of measured value for net water transport, which limits its use for the prediction of flooding. However, it could also be ascertained that even if

uncertainty exists over the net water transport, the model can still be used to obtain useful predictions on the oxygen mole fraction and flow velocity in the channel.

The modeling study was complemented with the experimental determination of net water transport. This was achieved by collecting water from the anode outlet with a drying agent. By comparing the amount of the collected water to the total water production, the fraction of water output through the anode was obtained. The results indicate that the variation of the net water transport coefficient across the active area needs to be considered for the accurate prediction of water transport in the cell. The effect of water redistribution by hydrogen flow was observed, indicating that the anode side flow geometry is an important design consideration in small fuel cells, where it is desirable to eliminate auxiliary devices that control water balance. It was found that when the general direction of the hydrogen flow was against the direction of the air flow, the distribution of water over the active area was more even than when the direction of hydrogen flow was the same as that of the air flow. The effect of anode conditions was also observed in a measurement series performed in dead-end mode, despite the lower flow rates of hydrogen.

The effect of ambient temperature and humidity on cell performance was analyzed by comparing data obtained under different ambient conditions. The comparison of data from different measurements at the upper end of the operating temperature range revealed that the onset of drying was affected by the vapor pressure of ambient air. Additional data on the effect of ambient conditions was available from measurements performed in a climate chamber. According to these results, the relative humidity of ambient air significantly affects the onset of flooding at the higher end of the studied ambient temperature range. In the measured current distributions, it could be seen that at a given average current density and cell temperature, the flooded region expanded downward in the channel as the relative humidity of ambient air was increased. At low overpotentials, the effect of the variation of ambient humidity on flooding was found to be small.

Stack research was included in the thesis with the investigation of ohmic losses in individual cells of a stack using the current interruption method. The ohmic losses of the unit cells were measured by observing the voltage transients in the unit cells with an oscilloscope. The detailed investigation of stacks at unit cell level is important, because large performance variations among unit cells will significantly decrease the overall power density of a stack. In addition, the peak current of the stack is determined by the weakest performing unit cell. A severe failure of one unit cell may even prevent the operation of the stack. The measurement of ohmic losses in the unit cells of a small stack revealed that in some cases, the middle cells of the stack were suffering from some local drying, which resulted from overheating. This was not obvious from the measurement of unit cell voltages.

As for the optimization of the cell design, the results of the work indicate water management as the most important area to be considered. Over most of the operating temperature range studied, the prevention of flooding at high current densities calls for attention. The removal of water would be facilitated by increasing the cross-section of the channels, which would increase the air flow rate and thus improve the removal of water in vapor form. The results also indicate that the increase of water vapor content over the length of the channels is relatively large at high current densities. It would be possible to increase the current density at which saturation at the upper end occurs by reducing the length of the channels and by increasing the number of parallel channels to

maintain the desired active area. For low operating temperatures, methods of removing the product water in liquid form may be worth considering, because the vapor pressure of water decreases with decreasing temperature, making it increasingly difficult to remove water in vapor form. In the prevention of drying at high current operating temperatures, the selection of the relative orientations of the air and hydrogen flows was found to be important. By redistributing the product water along with the hydrogen flow to the areas that are on the threshold of drying, the temperature at which the onset of drying occurs can be increased.

An optimized cell geometry may also place new requirements on the properties of the cell materials. In particular, increasing the width of the cathode channels or the ratio of channel width to rib width requires a more rigid gas diffusion material to be used. The results of a preliminary study indicate titanium sinters as a promising alternative to the traditionally used gas carbon-based materials. Furthermore, understanding the interaction of the gas diffusion layer material with water becomes increasingly important in the absence of the active control of water management, emphasizing the need for further research in this field.

The work as a whole provides a quantitative insight into mass transport phenomena in a natural convection fuel cell design with straight vertical cathode channels. The performance of the cell has been characterized by the measurement of current distribution, polarization, and resistance. The species mole fractions, air flow rate, and the net water transport coefficient have been quantified, and effects of ambient temperature and humidity have been measured. Based on the results, the driving forces of species transport and the performance limiting processes can be identified. The work has covered a broad range of operating conditions and current densities. The results obtained for this particular cell design can be generalized in the form of recommendations for the optimization of the design. The determination of an optimized design and the quantification of the resulting improvements are left for future work, but the results of the present study can be utilized to identify the relevant design parameters and to indicate the direction for optimization. Furthermore, a set of improved analysis tools is provided for future work on fuel cells.

References

[1] D. Swamy, “Battery availability: a true measure of mobile productivity”, in: *Commercialization of Small Fuel Cells & The Latest Battery Technologies for Portable Applications*, April 29-30, 1999, Bethesda, USA, The Knowledge Foundation, Inc., 1999.

[2] A.J. Appleby and F.R. Foulkes, *Fuel cell handbook*, New York, USA, van Nostrand Reinhold, 1989, 762 p., ISBN 00-442-31926-6.

[3] M. Rikukawa and K. Sanui, “Proton-conducting polymer electrolyte membranes based on hydrocarbon polymers”, *Prog. Polym. Sci.* **25** (2000) 1463-1502.

[4] V. Mehta and J.S. Cooper, “Review and analysis of PEM fuel cell design and manufacturing”, *J. Power Sources* **5044** (2002) 1-22.

[5] W. Liu, K. Ruth, and G. Rusch, “Membrane durability in PEM fuel cells”, *J. New Materials for Electrochem. Systems* **4** (2001) 227-231.

[6] M.S. Wilson and S. Gottesfeld, “Thin-film catalyst layers for polymer electrolyte fuel cell electrodes”, *J. Appl. Electrochem.* **22** (1992) 1-7.

[7] L.R. Jordan, A.K. Shukla, T. Bershing, N.R. Avery, B.C. Muddle, and M. Forsyth, “Diffusion layer parameters influencing optimal fuel cell performance”, *J. Power Sources* **86** (2000) 250-254.

[8] C. S. Kong, D.-Y. Kim, H.-K. Lee, Y.-G. Shul, and T.-H. Lee, “Influence of pore-size distribution of diffusion layer on mass-transport problems of proton exchange membrane fuel cells”, *J. Power Sources* **108** (2002) 185-191.

[9] Z. Qi and A. Kaufman, “Improvement of water management by a microporous sublayer for PEM fuel cells”, *J. Power Sources* **109** (2002) 38-46.

[10] E. Antolini, R.R. Passos, and E.A. Ticcianelli, “Effects of the carbon powder characteristics in the cathode gas diffusion layer on the performance of polymer electrolyte fuel cells”, *J. Power Sources* **109** (2002) 477-482.

[11] M. Mathias, J. Roth, J. Fleming, and W. Lehnert, “Diffusion media materials and characterization”, in: W. Vielstich, H.A. Gasteiger, and A. Lamm (eds.), *Handbook of fuel cells – Fundamentals, technology and applications*, Volume 3, John Wiley & Sons, Ltd., 2003.

[12] C. Zawodzinski and M.S. Wilson, “Metal screen and foil hardware for polymer electrolyte fuel cells”, in: S. Gottesfeld and T.F. Fuller (eds.), *Proton conductive membrane fuel cells II*, 1.-6.11. 1999, Boston, USA, The Electrochemical Society, Inc., *Electrochem. Soc. Proc.* Vol. **98-27**, 446-456, ISBN 1-56677-221-4.

[13] S. Gamburzev and A.J. Appleby, “Recent progress in performance improvement of the proton exchange membrane fuel cell (PEMFC)”, *J. Power Sources* **107** (2002) 5-12.

[14] A. Kumar and R.G. Reddy, “Modeling of polymer electrolyte membrane fuel cell with metal foam in the flow-field of the bipolar/end plates”, *J. Power Sources* **114** (2003) 54-62.

[15] S.O. Morner and S.A. Klein, “Experimental evaluation of the dynamic behavior of an air-breathing fuel cell stack”, *J. Solar Energy Engineering* **123** (2001) 225-231.

[16] P.-W. Li, T. Zhang, Q.-M. Wang, L. Schaefer, and M.K. Chyu, “The performance of PEM fuel cells fed with oxygen through the free-convection mode”, *J. Power Sources* **114** (2003) 63-69.

[17] F. Barbir, J. Braun, and J. Neutzler, “Effect of collector plate resistance on fuel cell stack performance”, in: S. Gottesfeld and T.F. Fuller (eds.), *Proton conductive membrane fuel cells II*, 1.-6.11. 1999, Boston, USA, The Electrochemical Society, Inc., *Electrochem. Soc. Proc.* Vol. **98-27**, 400-406, ISBN 1-56677-221-4.

[18] D.N. Busick and M.S. Wilson, “Low-cost composite bipolar plates for PEFC stacks”, in: S. Gottesfeld and T.F. Fuller (eds.), *Proton conductive membrane fuel cells II*, 1.-6.11. 1999, Boston, USA, The Electrochemical Society, Inc., *Electrochem. Soc. Proc.* Vol. **98-27**, 435-445, ISBN 1-56677-221-4.

[19] J. Scholta, B. Rohland, V. Trapp, and U. Focken, “Investigations on novel low-cost graphite composite bipolar plates”, *J. Power Sources* **84** (1999) 231-234.

[20] T.M. Besmann, J.W. Klett, J.J. Henry, Jr., and E. Lara-Curzio, “Carbon/carbon composite bipolar plate for proton exchange membrane fuel cells”, *J. Electrochem. Soc.* **147** (2000) 4083-4086.

[21] E. Middelman, W. Kout, B. Vogelaar, J. Lenssen, and E. De Waal, “Bipolar plates for PEM fuel cells”, *J. Power Sources* **118** (2003) 44-46.

[22] R.C. Makkus, A.H.H. Janssen, F.A. de Brujin, and R.K.A.M. Mallant, “Use of stainless steel for cost competitive bipolar plates in the SPFC”, *J. Power Sources* **86** (2000) 274-282.

[23] D.P. Davies, P.L. Adcock, M. Turpin, and S.J. Rowen, “Bipolar plate materials for solid polymer fuel cells”, *J. Appl. Electrochem.* **30** (2000) 101-105.

[24] D.P. Davies, P.L. Adcock, M. Turpin, and S.J. Rowen, “Stainless steel as a bipolar plate material for solid polymer fuel cells”, *J. Power Sources* **86** (2000) 237-242.

[25] N. Cunningham, D. Guay, J.P. Dodelet, Y. Meng, A.R. Hlil, and A.S. Hay, “New materials and procedures to protect metallic PEM fuel cell bipolar plates”, *J. Electrochem. Soc.* **149** (2002) A905-A911.

[26] J. Wind, R. Späh, W. Kaiser, and G. Böhm, “Metallic bipolar plates for PEM fuel cells”, *J. Power Sources* **105** (2002) 256-260.

[27] H. Wang, M.A. Sweikart, and J.A. Turner, “Stainless steel as bipolar plate material for polymer electrolyte membrane fuel cells”, *J. Power Sources* **115** (2003) 243-251.

[28] A. Schmitz, M. Tranitz, S. Wagner, R. Hahn, and C. Hebling, “Planar self-breathing fuel cells”, *J. Power Sources* **5213** (2003) 1-10.

[29] M.S. Wilson, “Annular feed air breathing fuel cell stack”, US Patent 5514486 (1996).

[30] J.K. Neutzler and M.S. Wilson, “Annular feed air breathing fuel cell stack”, US Patent 5595834 (1997).

[31] R. Jiang and D. Chu, “Stack design and performance of polymer electrolyte membrane fuel cells”, *J. Power Sources* **93** (2001) 25-31.

[32] H. Chang, J. R. Kim, J. H. Cho, H. K. Kim, and K. H. Choi, “Materials and processes for small fuel cells”, *Solid State Ionics* **148** (2002) 601-606.

[33] A. Heinzel, C. Hebling, M. Müller, M. Zedda, and C. Müller, “Fuel cells for low power applications”, *J. Power Sources* **105** (2002) 250-255.

[34] S.J. Lee, A. Chang-Chien, S.W. Cha, R. O’Hayre, Y.I. Park, Y. Saito, and F.B. Prinz, “Design and fabrication of a micro fuel cell array with ‘flip-flop’ interconnection”, *J. Power Sources* **112** (2002) 410-418.

[35] J.P. Meyers and H.L. Maynard, “Design considerations for miniaturized PEM fuel cells”, *J. Power Sources* **109** (2002) 76-88.

[36] J. Yu, P. Cheng, Z. Ma, and B. Yi, “Fabrication of a miniature twin-fuel-cell on silicon wafer”, *Electrochimica Acta* **48** (2003) 1537-1541.

[37] T.V. Nguyen, “A gas distributor design for proton-exchange-membrane fuel cells”, J. Electrochem. Soc. **143** (1996) L103-105.

[38] R. Mosdale and S. Srinivasan, “Analysis of performance and of water and thermal management in proton exchange membrane fuel cells”, *Electrochimica Acta* **40** (1995) 413-421.

[39] W.-K. Lee, C.H. Ho, J.W. van Zee, and M. Murthy, “The effects of compression and gas diffusion layers on the performance of a PEM fuel cell”, *J. Power Sources* **84** (1999) 45-51.

[40] H.-S. Chu, C. Yeh, F. Chen, “Effects of porosity change of gas diffuser on performance of proton exchange membrane fuel cell”, *J. Power Sources*, **123** (2003) 1-9.

[41] T. E. Springer, M. S. Wilson, and S. Gottesfeld, “Modeling and experimental diagnostics in polymer electrolyte fuel cells”, *J. Electrohem. Soc.* **140** (1993) 3513-3526.

[42] T.E. Springer, T.A. Zawodsinski, M.S. Wilson, and S. Gottesfeld, “Characterization of polymer electrolyte fuel cells using AC impedance spectroscopy”, *J. Electrochem. Soc.* **143** (1996) 587-599.

[43] Y.W. Rho, O.A. Velev, and S. Srinivasan, “Mass transport phenomena in proton exchange membrane fuel cells using O_2/He, O_2/Ar, and O_2/N_2 mixtures”, *J. Electrochem. Soc.* **141** (1994) 2084-2096.

[44] H. Dohle, A.A. Kornyshev, A.A. Kulikovsky, J. Mergel, and D. Stolten, "The current voltage plot of PEM fuel cell with long feed channels", *Electrochemistry Communications* **3** (2001) 73-80.

[45] A.A. Kulikovsky, "Performance of a polymer electrolyte fuel cell with long oxygen channel", *Electrochemistry Communications* **4** (2002) 527-534.

[46] A.A. Kulikovsky, "The voltage-current curve of a polymer electrolyte fuel cell: 'exact' and fitting equations", *Electrochemistry Communications* **4** (2002) 845-852.

[47] C. Haynes, "Clarifying reversible efficiency misconceptions of high temperature fuel cells in relation to reversible heat engines", *J. Power Sources* **92** (2001) 199-203.

[48] T.F. Fuller, J. Newman, "Experimental determination of the transport number of water in Nafion 117 membrane", *J. Electrochem. Soc.* **139** (1992) 1332-1337.

[49] T.A. Zawodsinski, C. Derouin, S. Radzinski, R.J. Sherman, V.T. Smith, T.E. Springer, S. Gottesfeld, "Water uptake by and transport through Nafion® membranes", *J. Electrochem. Soc.* **140** (1993) 1041-1047.

[50] T.A. Zawodzinski, J. Davey, J. Valerio, S. Gottesfeld, "The water content dependence of electro-osmotic drag in proton-conducting polymer electrolytes", *Electrochimica Acta* **40** (1995) 297-302.

[51] M. Ise, K.D. Kreuer, J. Maier, "Electro-osmotic drag in polymer electrolyte membranes: an electrophoretic NMR study", *Solid State Ionics* **125** (1999) 213-223.

[52] EG&G Technical Services, Inc., *Fuel Cell Handbook*, Sixth edition, Department of Energy, Office of Fossil Energy, National Energy Technology Laboratory, USA, 2002, DOE/NETL-2002/1179.

[53] J. Kaskimies, "Kaasuvirtaus polymeeripolttokennon katodilla (Gas flow on the cathode of a solid polymer fuel cell)", Helsinki University of Technology, 2000, Master's thesis (in Finnish).

[54] M. Noponen, "Experimental studies and simulations on proton exchange membrane fuel cell based energy storage systems", Helsinki University of Technology, 2000, Master's thesis.

[55] T. Mennola, "Design and experimental characterization of polymer electrolyte membrane fuel cells", Helsinki University of Technology, 2000, Licentiate's thesis.

[56] M. Mikkola, "Experimental studies on polymer electrolyte membrane fuel cell stacks", Helsinki University of Technology, 2001, Master's thesis.

[57] W.J. Wruck, R.M. Machado, and T.W. Chapman, "Current interruption – instrumentation and applications", *J. Electrochem. Soc.* **134** (1987) 539-546.

[58] C. Lagergren, G. Lindbergh, and D. Simonsson, "Investigation of porous electrodes by current interruption", *J. Electrochem. Soc.* **142** (1995) 787-797.

[59] F. N. Büchi, A. Marek, and G. Scherer, “In situ membrane resistance measurements in polymer electrolyte fuel cells by fast auxiliary current pulses”, *J. Electrochem. Soc.* **142** (1995) 1895-1901.

[60] F.N. Büchi and G.G. Scherer, “In-situ resistance measurements of Nafion® 117 membranes in polymer electrolyte fuel cells”, *J. Electroanalytical Chemistry* **404** (1996) 37-43.

[61] J.R. Selman and Y.P. Lin, “Application of ac impedance in fuel cell research and development”, *Electrochimica Acta* **38** (1993) 2063-2073.

[62] M. Ciureanu and R. Roberge, “Electrochemical impedance study of PEM fuel cells. Experimental diagnostics and modeling of air cathodes”, *J. Phys. Chem. B* **105** (2001) 3531-3539.

[63] B. Andreaus, A.J. McEnvoy, and G.G. Scherer, “Analysis of performance losses in polymer electrolyte fuel cells at high current densities by impedance spectroscopy”, *Electrochimica Acta* **47** (2002) 2223-2239.

[64] S.J.C. Cleghorn, C.R. Derouin, M.S. Wilson, and S. Gottesfeld, “A printed circuit board approach to measuring current distribution in a fuel cell”, *J. Appl. Electrochem.* **28** (1998) 663-672.

[65] J. Stumper, S.A. Campbell, D.P. Wilkinson, M.C. Johnson, and M. Davis, “In-situ methods for the determination of current distributions in PEM fuel cells”, *Electrochimica Acta* **43** (1998) 3773-3783.

[66] D.J.L. Brett, S. Atkins, N.P. Brandon, V. Vesovic, N. Vasileiadis, and A.R. Kucernak, “Measurement of the current distribution along a single flow channel of a solid polymer fuel cell”, *Electrochemistry Communications* **3** (2001) 628-632.

[67] N. Rajalakshmi, M. Raja, and K.S. Dhathathreyan, “Evaluation of current distribution in a proton exchange membrane fuel cell by segmented cell approach”, *J. Power Sources* **112** (2002) 331-336.

[68] E. Gülzow, T. Kaz, R. Reissner, H. Sander, L. Schilling, and M. v.Bradke, “Study of membrane electrode assemblies for direct methanol fuel cells”, *J. Power Sources* **105** (2002) 261-266.

[69] M.M. Mench and C.Y. Wang, “An in situ method for determination of current distribution in PEM fuel cells applied to a direct methanol fuel cell”, *J. Electrochem. Soc.* **150** (2003) A79-A85.

[70] M.M. Mench and C.Y. Wang, “Transient and steady state current density distribution measurements in a polymer electrolyte fuel cell”, to appear in: J.W. Van Zee, M. Murthy, T.F. Fuller, and S. Gottesfeld (eds.), *Proceedings of the 202nd meeting of the Electrochemical Society: Proton Conducting Membrane Fuel Cells III*, 20.-24.10. 2002, Salt Lake City, USA, The Electrochemical Society, Inc.

[71] Ch. Wieser, A. Helmbold, and E. Gülzow, “A new technique for two-dimensional current distribution measurements in electrochemical cells”, *J. Appl. Electrochem.* **30** (2000) 803-807.

[72] Y.-G. Yoon, W.-Y. Lee, T.-H. Yang, G.-G. Park, and C.-S. Kim, “Current distribution in a single cell of PEMFC”, *J. Power Sources* **118** (2003) 193.

[73] F.N. Büchi and S. Srinivasan, “Operating proton exchange membrane fuel cells without external humidification of the reactant gases”, *J. Electrochem. Soc.* **144** (1997) 2767-2772.

[74] G.J.M. Janssen and M.L.J. Overvelde, “Water transport in the proton-exchange-membrane fuel cell: measurements of the effective drag coefficient”, *J. Power Sources* **101** (2001) 117-125.

[75] D. Chu and R. Jiang, “Performance of polymer electrolyte membrane fuel cell (PEMFC) stacks Part I. Evaluation and simulation of an air-breathing PEMFC stack”, *J. Power Sources* **83** (1999) 128-133.

[76] R. Jiang and D. Chu, “Voltage-time behavior of a polymer electrolyte membrane fuel cell stack at constant current discharge”, *J. Power Sources* **92** (2001) 193-198.

[77] D.M. Bernardi and M. Verbrugge, “Mathematical model of a gas diffusion electrode bonded to a polymer electrolyte”, *AIChE J.* **37** (1991) 1151-1163.

[78] D.M. Bernardi and M. Verbrugge, “A mathematical model of the solid-polymer-electrolyte fuel cell”, *J. Electrochem. Soc.* **139** (1992) 2477-2491.

[79] T. E. Springer, T. A. Zawodzinski, and S. Gottesfeld, “Polymer electrolyte fuel cell model”, *J. Electrochem. Soc.* **138** (1991) 2334-2342.

[80] G. Murgia, L. Pisani, M. Valentini, and B. D’Aguanno, “Electrochemistry and mass transport in polymer electrolyte membrane fuel cells I. Model”, *J. Electrochem. Soc.* **149** (2002) A31.

[81] T.F. Fuller and J. Newman, “Water and thermal management in solid-polymer-electrolyte fuel cells”, *J. Electrohem. Soc.* **140** (1993) 1218-1225.

[82] T.V. Nguyen and R.E. White, “A water and heat management model for proton-exchange-membrane fuel cells”, *J. Electrochem. Soc.* **140** (1993) 2178-2186.

[83] V. Gurau, H. Liu, and S. Kakaç, “Two-dimensional model for proton exchange membrane fuel cells”, *AIChE J.* **44** (1998) 2410-2422.

[84] S. Um, C.-Y. Wang, and K.S. Chen, “Computational fluid dynamics modeling of proton exchange membrane fuel cells”, *J. Electrochem. Soc.* **147** (2000) 4485-4493.

[85] K. Dannenberg, P. Ekdunge, and G. Lindbergh, “Mathematical model of the PEMFC”, *J. Appl. Electrochem.* **30** (2000) 1377-1387.

[86] P. Futerko and I-M. Hsing, “Two-dimensional finite-element method study of the resistance of membranes in polymer electrolyte fuel cells”, *Electrochimica Acta* **45** (2000) 1741-1751.

[87] Z.H. Wang, C.Y. Wang, and K.S. Chen, “Two-phase flow and transport in the air cathode of proton exchange membrane fuel cells”, *J. Power Sources* **94** (2001) 40-50.

[88] D. Natarajan and T.V. Nguyen, “A two-dimensional, two-phase, multicomponent, transient model for the cathode of a proton exchange membrane fuel cell using conventional gas distributors”, *J. Electrochem. Soc.* **148** (2001) A1324-A1335.

[89] W. He, J.S. Yi, and T.V. Nguyen, “Two-phase flow model of the cathode of PEM fuel cells using interdigitated flow fields”, *AIChE J.* **46** (2000) 2053-2064.

[90] G.J.M. Janssen, “A phenomenological model of water transport in a proton exchange membrane fuel cell”, *J. Electrochem. Soc.* **148** (2001) A1313-A1323.

[91] L. You and H. Liu, “A two-phase flow and transport model for the cathode of PEM fuel cells”, *Int. J. Heat and Mass Transfer* **45** (2002) 2277-2287.

[92] T. Berning, D.M. Lu, and N. Djilali, “Three-dimensional computational analysis of transport phenomena in a PEM fuel cell”, *J. Power Sources* **106** (2002) 284-294.

[93] S. Shimpalee, “Numerical prediction of gas-humidification effects on energy transfer in pem fuel cells”, University of South Carolina, Columbia, 2001, Dissertation.

[94] S. Dutta, S. Shimpalee, and J.W. van Zee, “Numerical prediction of mass-exchange between cathode and anode in a PEM fuel cell”, *Int. J. Heat and Mass Transfer* **44** (2001) 2029-2042.

[95] A. Rowe and X. Li, “Mathematical modeling of proton exchange membrane fuel cells”, *J. Power Sources* **102** (2001) 82-96.

[96] M. Wöhr, K. Bolwin, W. Schnurnberger, M. Fisher, W. Neubrand, and G. Eigenberger, “Dynamic modeling and simulation of a polymer membrane fuel cell including mass transport limitation”, *Int. J. Hydrogen Energy* ***2*****3** (1998) 213-218.

[97] N. Djilali and D. Lu, “Influence of heat transfer on gas and water transport in fuel cells”, *Int. J. Therm. Sci.* **41** (2002) 29.

[98] M. Roos, E. Batawi, U. Harnisch, and Th. Hocker, “Efficient simulation of fuel cell stacks with the volume averaging method”, *J. Power Sources* **118** (2003) 86-95.

[99] R.J. Bellows, M.Y. Lin, M. Arif, A.K. Thompson, and D. Jacobson, “Neutron imaging technique for in situ measurement of water transport gradients within Nafion in polymer electrolyte fuel cells”, J. Electrochem. Soc. **146** (1999) 1099-1103.

[100] D. Webb and S. Møller-Holst, “Measuring individual cell voltages in fuel cell stacks”, *J. Power Sources* **103** (2001) 54-60.

[101] T. Hottinen, private communication, 2003.